Cell Reports
Sustainability

Article

A theoretical upper limit for offshore wind energy extraction

Graphical abstract

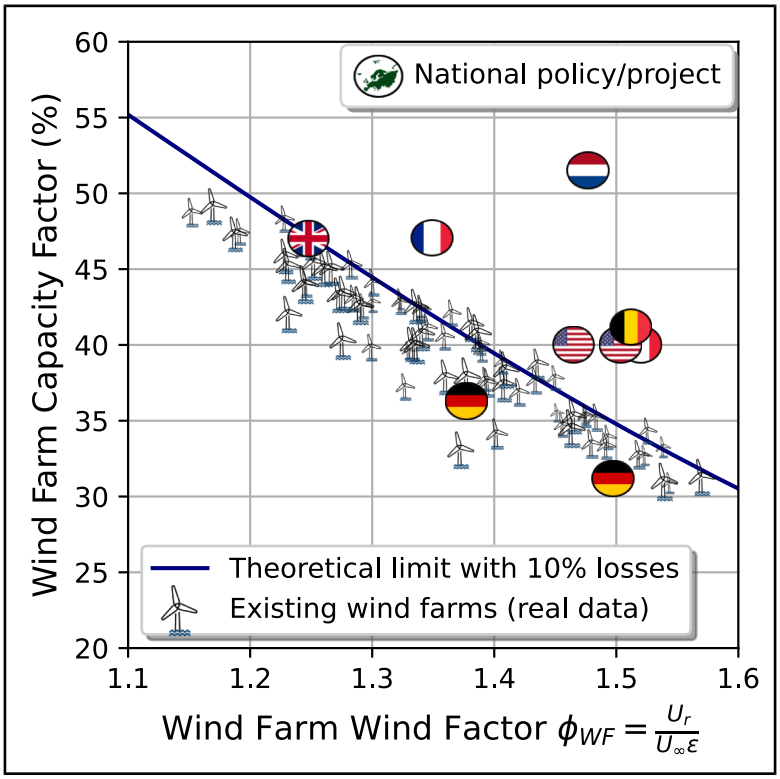

Highlights

- Defines the aerodynamic upper limit of offshore wind energy production
- Validated with 72 offshore wind farms over 420 cumulative operational years
- National policy targets overestimate energy production output by up to 50%
- Provides a simple tool usable across disciplines to set realistic targets

Authors

Carlos Simão Ferreira,
Gunner Chr. Larsen,
Jens Nørkær Sørensen

Correspondence

c.j.simaoferreira@tudelft.nl (C.S.F.),
gula@dtu.dk (G.C.L.),
jnso@dtu.dk (J.N.S.)

In brief

Simão Ferreira et al. present a validated analytical model that defines the physical upper limit of offshore wind farm production. Using data from 72 farms over 420 years of operation, the study shows that national policy targets often overestimate output by up to 50%. The model provides policymakers and planners with a simple, cross-disciplinary tool to set realistic energy goals, highlighting the need for credible planning to safeguard society's transition to clean power.

Simão Ferreira et al., 2026, Cell Reports Sustainability *3*, 100573
January 23, 2026
https://doi.org/10.1016/j.crsus.2025.100573

CellPress

Cell Reports Sustainability

CellPress
OPEN ACCESS

Article

A theoretical upper limit for offshore wind energy extraction

Carlos Simão Ferreira,[1,4,*] Gunner Chr. Larsen,[2,*] and Jens Nørkær Sørensen[3,*]
[1]Faculty Aerospace Engineering, Delft University of Technology, Kluyverweg 1, 2629 HS Delft, the Netherlands
[2]Response, Aero-elasticity, Control and Hydrodynamics, DTU Wind, Frederiksborgvej 399, 4000 Roskilde, Denmark
[3]Section of Aero- and Fluid Dynamics, DTU Wind and Energy Systems, Nils Koppels Allé, bldg. 403, 2800 Lyngby, Denmark
[4]Lead contact
*Correspondence: c.j.simaoferreira@tudelft.nl (C.S.F.), gula@dtu.dk (G.C.L.), jnso@dtu.dk (J.N.S.)
https://doi.org/10.1016/j.crsus.2025.100573

SCIENCE FOR SOCIETY Offshore wind energy is key to energy transition, but its true potential is often overstated. As wind farms become larger and denser, they change the atmospheric boundary layer, reaching up to the strong geostrophic winds a few kilometers above the surface. Energy extraction depends on the vertical transfer of momentum from these high-altitude winds down to the turbines, which sets a physical ceiling on how much energy can harvested. A closed-form analytical model, validated against more than 420 years of operational data from 72 wind farms, defines this upper limit through a dimensionless Wind Farm Wind Factor, which condenses the key design and operational conditions of the wind farm, turbine, and site. A benchmark of national policy targets shows expectations of energy production up to 50% higher than can realistically be achieved. Such overestimation not only hides true energy costs but also underestimates power variability, integration, and curtailment risks, and it distorts policy pathways. When projections exceed physical limits by such margins, the resulting electricity shortfall can destabilize decarbonization strategies and reach deep into society and the economy. Because of the long lead times to develop projects and new electricity systems including storage and the long operational life of these assets, errors in projections will affect multiple generations. The heavy demands on society (e.g., qualified labor), the economy, and the environment mean that corrective paths may become costly or unfeasible for a country or region. The framework provides policymakers, planners, and communities with a rigorous yet simple tool to set credible targets; compare technology choices; and balance trade-offs between space use, biodiversity, and energy security. It also enables collaboration across engineering, economics, and environmental sciences, helping to deliver on climate goals without overpromising or undermining trust in energy transition.

SUMMARY

Future energy systems need offshore wind. However, large-scale deployment faces aerodynamic limits that constrain efficiency, energy yield, and grid integration. We present a closed-form analytical model for the theoretical upper limit to offshore wind farm production, expressed through a dimensionless Wind Farm Wind Factor. The model and limit are validated against data from 72 offshore wind farms over 420 cumulative years, demonstrating strong agreement including operational losses. We benchmark national policy targets in Europe and the US, revealing large overestimations of energy production—by nearly 50% in one case—underestimating energy costs, power variability and integration costs, curtailment, and policy risks. The model clarifies the critical design trade-offs between turbine height, specific power, and wind farm density. Our model provides a rigorous yet simple framework, readily usable by engineers, planners, and policymakers to forecast wind farm performance, support system planning, and to set realistic targets consistent with aerodynamic limits.

INTRODUCTION

Offshore wind energy is a crucial component in the pursuit of carbon neutrality by coastal nations. It is projected that by 2050, global offshore wind capacity will reach approximately 1,800 GW.[1] This expansion will constitute about 80% of all marine space utilization by fixed structures, including both energy and non-energy infrastructure.[1] The development of offshore wind

farms involves extensive planning and construction phases, with operational lifespans exceeding 25 years. Offshore wind now accounts for over 50% of all capital investments in marine industries.[1] However, the inherent variability of wind energy, combined with its increasing market penetration, presents substantial challenges for system integration, necessitating major infrastructural enhancements.[2–6]

The growth of the offshore wind sector demands enduring policy support and will have profound societal and environmental impacts that extend across several decades and affect multiple generations of people and wildlife. The industry's operation, characterized by high volumes and narrow profit margins, is particularly sensitive to global fluctuations in material and energy costs.[7] Project forecasts and transnational policy decisions are based on a range of models and assumptions with significant uncertainty.[8–12]

It is essential for governments, regulatory bodies, industry stakeholders, financial institutions, and community representatives to have access to reliable energy production forecasts from wind farms. These energy production forecast models should be openly accessible, straightforward to interpret and use, and subject to transparent validation processes.

The aim of this work is to provide and validate a simple closed-form analytical model to predict wind farm energy production based on the physics of wind farm interactions with the atmospheric boundary layer (ABL). The core model has been previously developed by Frandsen[13] and extended by Sørensen and Larsen.[14] We validate the model against historical production data of over 70 offshore wind farms located in the Baltic, North, and Irish Seas for a total of more than 420 years of data.

We further extend the model by deriving a new theoretical upper limit for the production of a wind farm, and we validate it with full-scale wind farm data, with most wind farms already performing at below and around 90% of the new proposed theoretical maximum, explained by the operational losses. This theoretical limit is rigorously defined for infinite wind farms by physical principles. For real wind farms, a small empirical correction is needed to account for the enhanced production of edge turbines, but this does not affect the theoretical ceiling itself.

Leveraging this validated approach, we then analyze several planned large-scale offshore wind projects and national policy targets. Comparing their published capacity factors against our theoretical limit reveals that many official goals are overly optimistic by as much as 50%. This discrepancy not only affects feasibility but also has implications for levelized cost of energy (LCOE) estimates and system integration planning. Lastly, we explore how the model's findings relate to turbine design choices, wind farm density, and variability in power output, offering insights that are directly applicable to both industry and policymakers.

RESULTS AND DISCUSSION

Validation of model with wind farm data

In this section, we validate the wind farm model by comparing its predictions of capacity factor (*CF*)—the ratio of a wind farm's average power output to its nameplate capacity—against real-world data from operational wind farms. The details of the model formulation and data sources are provided in the methods and in Simão Ferreira.[15]

Figure 1 presents the geographic locations of 72 offshore wind farms in the Baltic, North, and Irish Seas (the background map is adapted from European Marine Observation and Data Network [EMODnet],[16] which includes wind farms up until the planning phase. For reference on wind farms up until the exploration phase, see 4C Offshore[17]). The distribution of installed capacity (MW) and wind farm capacity density (MW/km^2) is depicted in Figure 2. These datasets provide the basis for model validation.

Figure 3 provides a direct comparison of the capacity factor predicted by the model and the capacity factor from real wind farm data. The model estimates for capacity factor account only for wake losses, excluding operational factors such as availability, grid constraints, maintenance, and transmission losses. In contrast, real wind farm data represent the energy delivered to the grid, incorporating all operational losses.

Typical operational losses of offshore wind farms range from approximately 10% of the potential production after wake losses,[18,19] with some studies suggesting values as high as 14%.[20] As shown in Figure 3, most real-world capacity factors fall between 85% and 95% of the model predictions, with an average ratio of 89%, aligning well with expected operational losses.

A linear regression of the dataset, using the form $y = 0.89x$, where y shows the capacity factors of the real wind farms and x represents capacity factor predicted by the model, yields a coefficient of determination $R^2 = 0.87$. This indicates a strong correlation between model predictions and real-world performance.

However, some data points deviate from this trend. When observing the specific data points, these deviations are often due to factors such as wind farm-specific curtailments, additional wake effects from neighboring wind farms, or seasonal variations in wind resource availability.

This validation demonstrates that the model effectively captures the aerodynamic behavior of offshore wind farms while closely approximating real-world performance, reinforcing its utility for forecasting the production of offshore wind farms.

In the simulations corresponding to Figure 3, the effects of finite wind farm size, layout, wind farm aspect ratio, and orientation relative to the prevailing wind distribution are addressed by partitioning the turbines; a subset is assigned to experience unperturbed wind speeds (without wind farm reduction effects), while the remaining turbines experience the full velocity reduction inside an infinite wind farm (see section on definition of the Wind Farm Wind Factor). All parameters used for the simulation of each wind farm, along with the corresponding historical production data, are provided in the database[15] and can be freely downloaded for verification and further analysis.

Validation of the theoretical limit for energy extraction

This section presents the validation of the equations presented in the methods for the theoretical limit for energy extraction.

The Wind Farm Wind Factor, ϕ_{WF}, is defined as the ratio of the turbine rated wind speed (U_r) to the product of the unperturbed mean wind speed at hub height (U_∞) and the velocity reduction factor (ϵ), which accounts for the impact of wind farm layout

CellPress
OPEN ACCESS

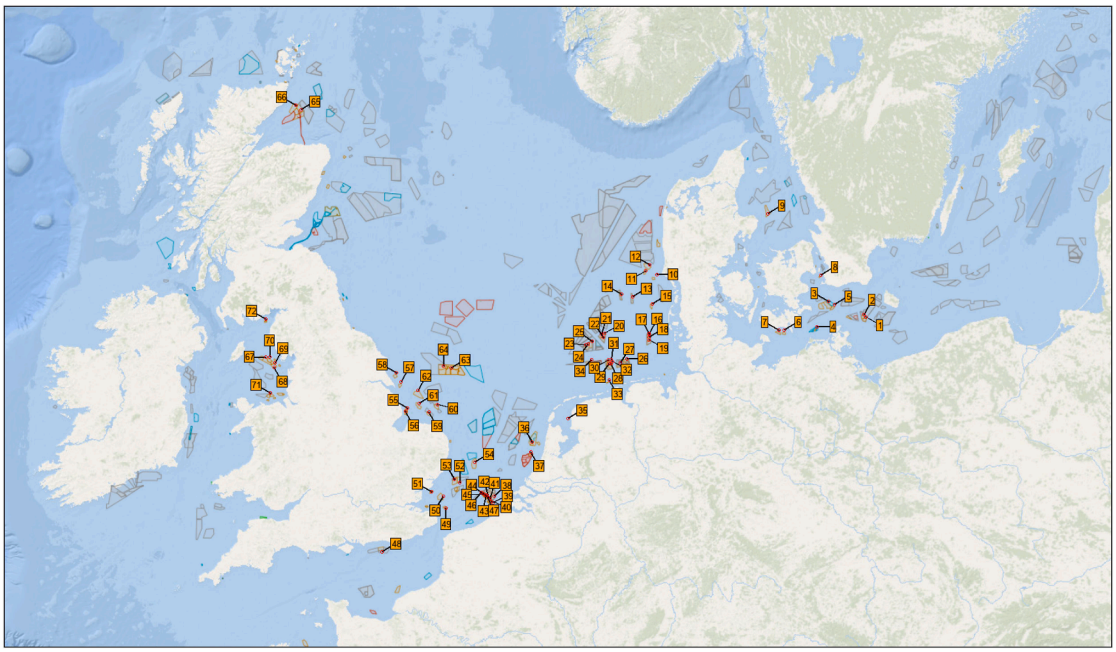

Figure 1. Geographic locations of wind farms in the Baltic, North, and Irish Seas

Labels correspond to those in Figure 2, and the data points are described in Simão Ferreira.[15] Background map adapted from European Marine Observation and Data Network.[16]

and wake effects. This dimensionless parameter condenses the essential influences of turbine design, site wind resource, and farm configuration into a single value (see methods for detailed derivation).

Figure 4 shows the capacity factor as a function of the Wind Farm Wind Factor $\phi_{WF} = \frac{U_r}{U_\infty \epsilon}$, where the data points represent the real wind farm data. The data points account for the equivalent value of the velocity reduction factor ϵ, as introduced in Sørensen and Larsen[14] for a *finite* wind farm, which accounts for the fact that the first rows of the wind farm experience unperturbed flow. Two lines are drawn—the theoretical limit line for k = 2.4, as given by Equation 11, and the theoretical limit line accounting for 10% losses (90% of the theoretical limit), which is consistent with empirical values listed in Mortensen.[18] The theoretical limit assumes a cut-in wind speed of 0 m/s and a cut-out wind speed of $\infty m/s$, while the wind farm simulations assume a cut-in wind speed of 3 m/s and a cut-out wind speed of 25 m/s. The real wind farm data follow slightly below the 90% theoretical limit line. This attests that most wind farms are already designed to operate close to the practical maximum, even though designers may not have been aware of this limit.

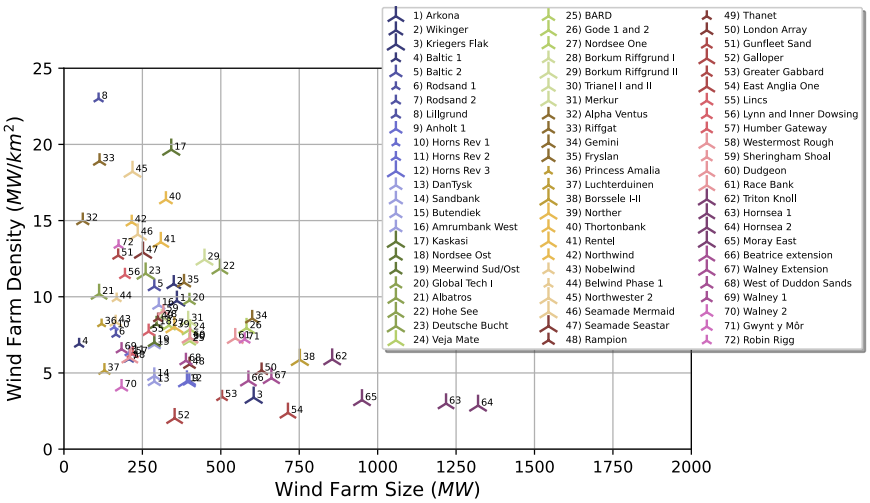

Figure 2. Distribution of wind farm installed capacity (MW) and wind farm capacity density (MW/km^2) in the dataset

Marker size is proportional to rotor diameter. Labels correspond to those in Figure 1, and the data points are described in Simão Ferreira.[15]

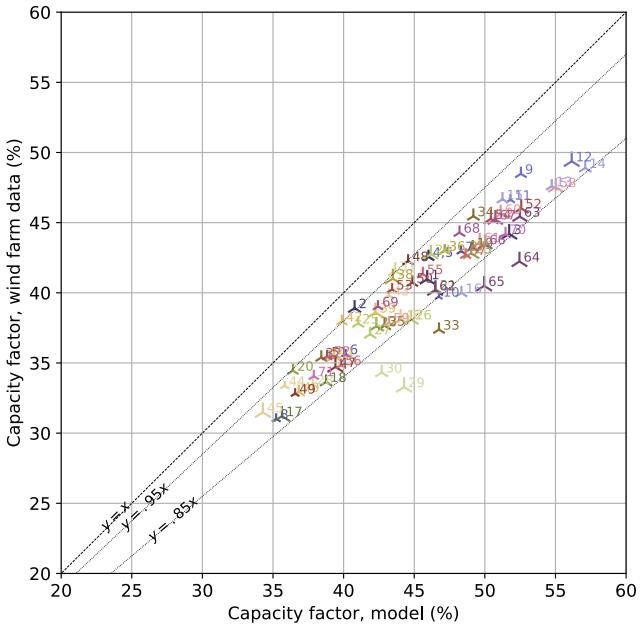

Figure 3. Comparison of capacity factor estimates from the model (energy extraction, no operational losses) versus real wind farm data (operational losses included)

The diagonal reference lines indicate 100%, 95%, and 85% agreement. Labels correspond to those used in Figures 1 and 2, and the data points are described in Simão Ferreira.[15]

The proposed theoretical limit is therefore validated by the real wind farm data. Despite being simple, the closed-form equation is capable of capturing the essential physical processes that determine the energy yield.

Referring to Figure 4, it is clear that the Wind Farm Wind Factor is an efficient predictive measure of the highest achievable wind farm capacity factor for a given wind farm layout and for given site conditions (expressed in terms of geostrophic wind conditions, the ground roughness height, and the Coriolis parameter). Both site wind speed conditions and the wind farm topology are condensed into the ϵ parameter defined in Equation 6, which expresses the ratio between the wind speed within the infinite wind farm and the unperturbed ambient wind speed at hub height.

For given site conditions, the impact of wind farm layout on the achievable wind farm capacity factor is expectedly intimately related to the wind farm density. For small turbine spacing—i.e., large turbine density—the Wind Farm Wind Factor increases, resulting in a decrease in the obtainable wind farm capacity factor. In the limit of infinite spacing, ϵ approaches 1, and the Wind Farm Wind Factor takes its maximum equal to $\frac{U_r}{U_\infty}$ and thus degenerates to the *turbine* wind factor.

Evaluation of national offshore wind policies

Establishing an analytical upper limit to the capacity factor of offshore wind farms offers a significant advantage; it can serve as a robust tool to enhance decision-making and governance processes. This includes the strategic planning and negotiation phases, as well as the definition of offshore leases and the setting of wind energy tariffs. Current national policies are typically informed by diverse studies employing varied tools and methodologies.

The feasibility of national offshore wind policies and projects was evaluated using the theoretical capacity factor limits derived in this study. The policy goals and planned projects for selected countries were assessed by comparing published targets with the calculated capacity factor limits and operational constraints. Detailed descriptions of the case studies, including wind farm parameters and data sources, are provided in the section on descriptions of case studies of policy goals. This section focuses on analyzing the alignment of policy ambitions with theoretical and practical constraints, highlighting discrepancies and implications for offshore wind energy development.

The evaluation included the following national policy case studies, which are presented using their names and acronyms:

- UK: Hornsea 3 (UK North Sea).

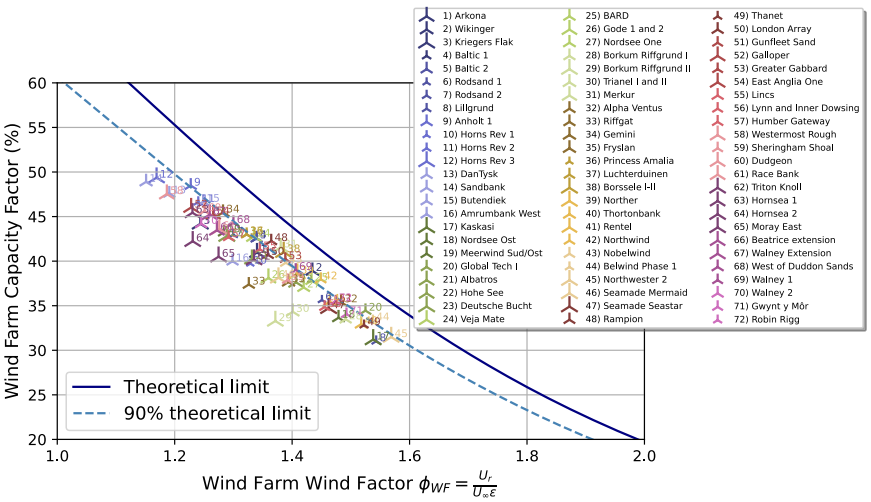

Figure 4. Relationship between wind farm wind factor $\phi_{WF} = \frac{U_r}{U_\infty \epsilon}$ and wind farm capacity factor *CF* (%)

The data points represent the individual wind farms. The theoretical limit line for Weibull shape factor k = 2.4 and the theoretical limit line accounting for 10% losses are also shown. Labels correspond to those used in Figures 1 and 2, and the data points are described in Simão Ferreira.[15]

Table 1. Comparison of wind farm data for national policy/project study cases as described

Case study –	Capacity installed (MW)	Capacity density (MW/km^2)	U_∞ @150m (m/s)	WFWF Φ_{WF} (–)	CF policy (%)	CF theory (%)	CF policy / CF theory (%)	Power density (MW/km^2)
UK	2,955	4.2	10.2	1.25	47.0	46.1	102	2.0
FR 1	2,497	5.5	9.4	1.35	47.1	40.9	115	2.3
DE 1	12,000	10.4	10.5	1.38	36.3	39.4	92	4.1
US 1	2,837	6.9	9.5	1.46	40.0	35.2	113	2.4
NL	10,000	10.0	10.0	1.48	51.5	34.6	149	3.5
DE 2	5,500	13.1	10.3	1.50	31.1	33.7	93	4.4
US 2	9,646	6.8	9.5	1.50	40.0	33.5	120	2.3
BE	3,500	13.7	9.7	1.51	41.2	33.1	124	4.5
FR 2	1,200	6.7	8.3	1.52	40.0	32.7	122	2.2

The table includes installed capacity (MW), capacity density (MW/km^2), unperturbed wind speed at height 150 m (m/s), calculated Wind Farm Wind Factor (ϕ_{WF}), capacity factor from policy/project goals presented in literature (CF_{policy}), calculated theoretical capacity factor (CF_{theory}) with 10% operational losses, the ratio of policy capacity factor to the theoretical limit (CF_{policy}/CF_{theory}), and effective average power density (MW/km^2). The results illustrate significant discrepancies between policy/project goals and theoretical constraints for some cases (see also Figure 5)

- FR 1: Centre Manche I and II (Channel Region, France).
- FR 2: Oléron I (Atlantic Coast, France).
- DE 1: N9 Zone (German North Sea).
- DE 2: N11–13 Zone (German North Sea).
- US 1: Atlantic Shores South (United States, Atlantic Coast).
- US 2: New York Bight (United States, Atlantic Coast).
- NL: North Sea Programme (Dutch North Sea).
- BE: Princess Elisabeth Zone (Belgian North Sea).

These cases were selected to provide a representative overview of national ambitions across various offshore wind energy contexts. Selection was based on the availability and specificity of public data and definitions, as well as on the size and relevance of the projects. This ensures that each case represents a clearly defined, high-impact national or regional initiative for which detailed parameters are available. Results are presented in terms of alignment with theoretical limits, in some cases highlighting significant discrepancies between policy goals and achievable capacity factors.

Table 1 presents a comparison of national policy and project case studies for offshore wind farms, highlighting critical parameters such as installed capacity, capacity density, wind speed, and capacity factors. The table contrasts the published capacity factor goals (CF_{policy}) with theoretical limits (CF_{limit}) derived from this study, accounting for 10% operational losses. For six cases, the ratio is above 111%, representing policy goals above the theoretical limits without operational losses. The ratio CF_{policy}/CF_{limit} quantifies the degree of alignment between the policy ambitions and theoretical constraints, while the power density (average power produced per unit area) provides insight into spatial efficiency for energy production. The average wind speed is retrieved from Technical University of Denmark.[21]

Figure 5 illustrates the relationship between the Wind Farm Wind Factor (ϕ_{WF}) and the capacity factor, comparing existing wind farms with national policy cases. The theoretical capacity factor limit (navy-blue solid line) and adjusted limit for operational losses (blue dashed line) are shown. Circle-shaped markers represent policy or project goals. Star-shaped markers indicate expected capacity factors at 90% of the theoretical limit but are calculated specifically over the operational wind speed range of the turbine (3–25 m/s), rather than the full wind speed range. The blue dashed line, in contrast, represents 90% of the theoretical upper limit computed over the entire wind speed range from 0 to infinity. The data points from the operational wind farms align closely with the 90% markers, supporting the validity of the model.

The results reveal significant discrepancies between some policy goals and theoretical limits. Several national policies/projects target capacity factors and densities that exceed realistic constraints, as evidenced by the position of circle markers above the theoretical limit lines in Figure 5 (even above the absolute theoretical limit, where no operational losses are assumed). These discrepancies highlight potential overestimations in planning, which could impact the feasibility of policy, the societal and economic value, and the integration in the energy system.

The Dutch policy case is particularly instructive, not only because it represents the largest observed mismatch between official targets and aerodynamic limits but also because it illustrates how policy can rapidly evolve, sometimes in counterproductive directions. Policy is inherently dynamic, and the recent developments in the Netherlands—including the updated *Windenergie Infrastructuurplan Noordzee* (WIN) and its accompanying parliamentary letter published on July 16, 2025 (*Kamerbrief Het Windenergie Infrastructuurplan Noordzee*[22] and *Bijlage Het Windenergie Infrastructuurplan Noordzee*[23])—provide a case study of how changing targets, spatial planning, and assumed performance can become misaligned with physical constraints.

In the Dutch case, national planning assumptions for offshore wind have shifted from 10 MW/km^2 and a capacity factor of 51.5% (as in the North Sea Programme 2022–2027[19,24–27]) to the latest government plan targeting 10.5 MW/km^2 and even higher capacity factors —ranging from 51% to 56%. However, these scenarios are not only internally inconsistent with physical wake losses at higher densities, but they also depart from observed trends in operational wind farms. The WIN plan itself

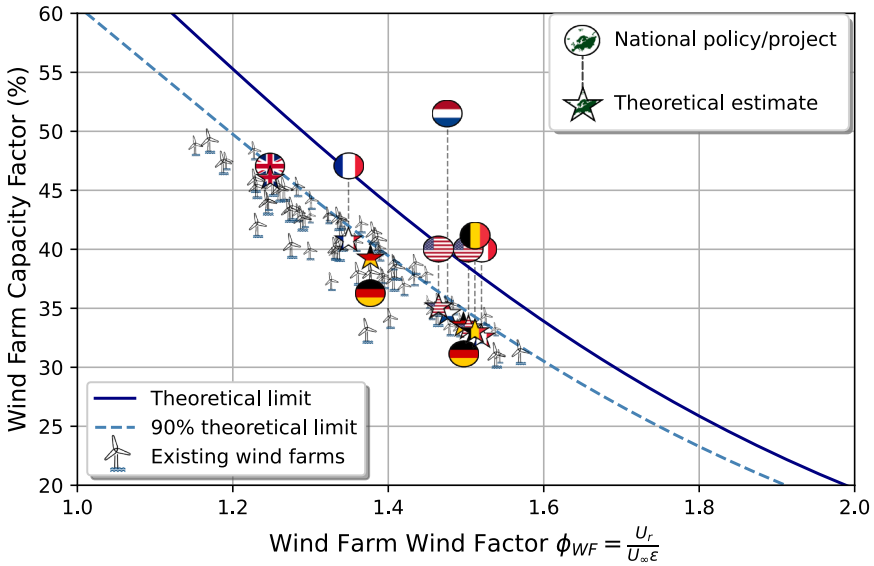

Figure 5. Relationship between the Wind Farm Wind Factor ($\phi_{WF} = U_r/U_\infty\epsilon$) and the wind farm capacity factor (%)

For a Figure360 author presentation of this figure, see https://doi.org/10.1016/j.crsus.2025.100573. Figure360▷

The theoretical limit (navy-blue solid line) and the adjusted limit accounting for 10% operational losses (blue dashed line) are shown alongside data points representing existing offshore wind farms (see also Figure 4) and national policy cases. Circle-shaped markers indicate the published goals of national policies/projects, while star-shaped markers represent the theoretical estimate with 10% operational losses. The results show that several national policies/projects are significantly above the theoretical limit, highlighting potential overestimations in planning. The results are also expressed in Table 1.

acknowledges in its technical appendix that such high capacity factors may be optimistic. Indeed, only a single scenario variant models a lower capacity factor of 42% (3,700 full load hours) yet frames it as "pessimistic." The simultaneous assumption of both higher densities and rising capacity factors is not physically plausible, as increased capacity density is aerodynamically linked to a lower, not higher, average capacity factor. The result is a policy trajectory that, without adjustment, risks significantly overstating potential energy yields, underestimating integration costs, and misaligning spatial planning with achievable system performance. For these reasons, our analysis employs the more conservative values from the original North Sea Programme,[19,24–27] and we recommend that future planning scenarios should reflect the realistic trade-off between farm density and achievable capacity factor.

This risk becomes especially acute when quantifying the actual gap that emerges if offshore wind CFs are overestimated. The WIN plan, for example, assumes that offshore wind will provide around 60% of all CO_2 -free electricity generated in the Netherlands by 2040, based on capacity factors as high as 53% (in average). If, instead, the system-average capacity factor proves to be closer to 34.6%—as predicted by our theoretical model and supported by global operational trends—then more than 20% of the Netherlands' planned CO_2 -free electricity supply will be missing by 2040 due to the shortfall in offshore wind generation alone. To put this in perspective, this lost share is equivalent to the entire projected output of solar photovoltaics in the WIN plan,[23] nearly twice the expected contribution from onshore wind, and almost three times the nuclear energy output anticipated in 2040. Such a discrepancy would fundamentally threaten the viability and credibility of the Dutch decarbonization pathway.

Even when assuming CFs above 50%, the Dutch government's own scenario analysis acknowledges that massive new investments in grid infrastructure, energy storage, and flexible demand are indispensable to avoid curtailment and system bottlenecks. The WIN report[23] notes that as renewable shares rise above 70%–80%, only large-scale solutions such as hydrogen production, grid expansion, and both short- and long-term storage can enable further integration. Without these, the system cannot reach its renewable targets, regardless of assumed wind performance.

It is also important to note that the feasibility and cost-effectiveness of the large-scale storage and flexibility investments envisioned by Dutch policy critically depend on the actual capacity factor of the wind fleet. If, as aerodynamic limits and operational experience suggest, average offshore wind capacity factors fall well below 50%, the utilization rate of storage and flexible demand assets will be much lower than assumed. This not only drives up the levelized cost of stored (or converted) energy, but it also undermines the ability of these systems to provide reliable grid support, amplifying the risk of underdelivery and economic inefficiency. In other words, planning for very high levels of offshore wind integration without realistic capacity factor assumptions may significantly overstate the benefits—and understate the costs—of storage, hydrogen, and system integration solutions. This analysis highlights the critical importance of aligning national targets and infrastructure planning with empirically grounded, physically realistic performance limits for offshore wind energy. Furthermore, it underscores the urgency of immediate dissemination and education regarding the theoretical and empirical limits of offshore wind energy. When we began this work over 2 years ago, the Dutch targets were already overly optimistic; since then, policy assumptions have only drifted further from physical reality, amplifying the risks of overpromise and underdelivery.

The US offshore wind case studies (*US 1*: Atlantic Shores South, *US 2*: New York Bight) illustrate a distinct challenge in translating policy assumptions into project realities. Both projects initially adopted an assumed capacity factor of 40%, as calculated by the Bureau of Ocean Energy Management (BOEM) during the leasing phase, based on a conservative capacity density of 3 MW/km^2 (see Bureau of Ocean Energy Management,[28] *Lease Area Descriptions*). At this lower density, our

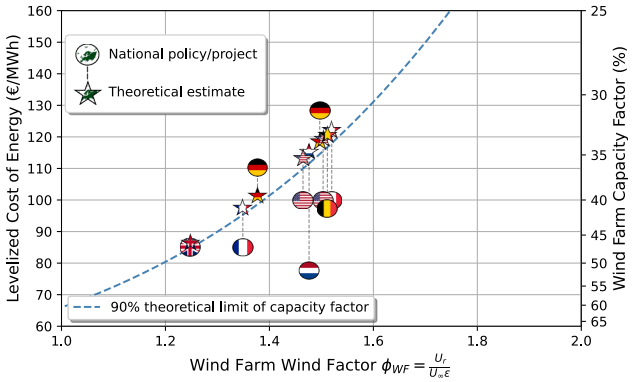

Figure 6. LCOE as a function of the Wind Farm Wind Factor (ϕ_{WF}) and wind farm capacity factor (%)

The blue dashed-line represents the LCOE trend assuming an inverse proportionality to CF with a reference cost of 80€/MWh at $CF = 50\%$, and CF is 90% of the theoretical capacity factor limit. Circle-shaped markers indicate the estimates of LCOE based on the capacity factor published as goals of national policies/projects, while star-shaped markers represent the expected values of LCOE based on the capacity factor obtained from the model, as shown in Figure 5 and Table 1.

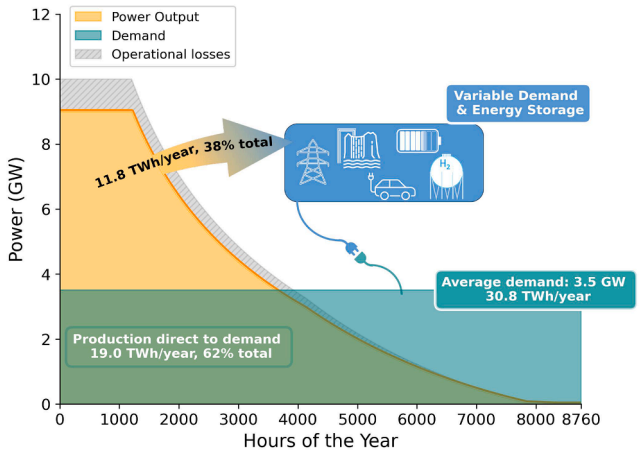

Figure 7. Ordered annual power-output distribution for a hypothetical 10 GW offshore wind farm with a capacity factor $CF = 35\%$

Colored regions indicate production above the mean power level. Curved arrows show what fraction of total annual energy is produced above this baseline, highlighting the need for flexible demand or energy storage. The example assumes no storage or curtailment losses. Turbine rated wind speed is $U_r = 10.5 m/s$, average unperturbed wind speed at hub height $h = 150m$ is $U_\infty = 10 m/s$, and the Weibull shape factor is $k = 2.4$.

analytical model predicts capacity factors of 43.3% for *US 1* and 41.6% for *US 2*—slightly above BOEM's original estimate and confirming its initial reasonableness. Notably, BOEM had already acknowledged during the leasing process that actual projects would likely be developed at higher densities. Indeed, the final designs for *US 1* and *US 2* reached 6.9 and 6.8 MW/km^2, respectively—more than double the original planning assumption. Nevertheless, the policy and publicly communicated capacity factor have remained fixed at 40%, with no adjustment for the increased aerodynamic losses associated with such dense layouts. This disconnect highlights a failure to update initial leasing-phase assumptions in response to project-level changes, resulting in unrealistic and overly optimistic expectations for the ultimate energy yield of these higher-density projects.

Impact on cost of energy

In this section, we evaluate the LCOE across different national offshore wind policies, using the capacity factor estimates derived in the previous section. The methodology for LCOE estimation is detailed in the section on LCOE estimation methodology. Our model treats capacity factor as the sole variable in determining the LCOE, assuming that all other cost drivers remain constant.

Figure 6 presents the relationship between LCOE and the Wind Farm Wind Factor (ϕ_{WF}) and the associated capacity factor. The blue dashed line represents the LCOE trend assuming an inverse proportionality to CF with a reference cost of 80€/MWh at $CF = 50\%$, and CF is 90% of the theoretical capacity factor limit. Circle markers indicate LCOE estimates based on policy-reported CFs, while star markers represent expected LCOE values assuming CFs estimated by the model. For comparison with the estimates, the work of Fuchs et al.[20] shows an average 167 USD/MWh (162 €/MWh) of requested strike price for projects in the same region as the case studies *US 1* and *US 2*.

These results indicate that overestimating a wind farm's capacity factor leads to an overestimation of its energy output and, consequently, to an underestimation of the cost of energy. Because the calculated LCOE is inversely proportional to the capacity factor (Table 1), even modest capacity factor errors can significantly affect project feasibility. This issue is particularly relevant given the long intervals between initial site studies by governmental bodies, formal project tenders, and actual construction.

Impact on the variability of power produced

A central challenge with variable renewable energy is that production cannot be provided at will but only when sufficient wind is available. Consequently, a wind farm capacity factor not only denotes the average power output during its lifetime, but it also reflects how the energy is distributed throughout the year.

Figure 7 illustrates this distribution for a hypothetical 10 GW offshore wind farm at a capacity factor of $CF = 35\%$. The hours are sorted in descending order of power output, revealing that much of the yearly energy is produced in relatively few hours. If the goal were to supply a near-constant baseline of power, the system would need flexible demand and/or storage, managing close to 40% of the energy produced. In this idealized example, we assume zero curtailment losses, zero storage losses, and no losses from variable demand.

Because the Wind Farm Wind Factor ϕ_{WF} determines the farm's capacity factor, we can also track how the distribution of output changes with ϕ_{WF}. Figure 8 plots the fraction of hours spent at various power levels versus increasing ϕ_{WF}. As ϕ_{WF} grows (and CF drops), the power-duration curve becomes more concave—a larger share of total energy is produced in fewer high-output hours, leaving more hours at minimal output.

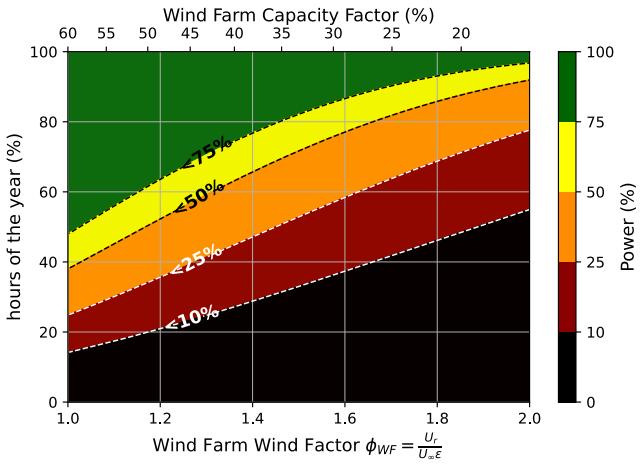

Figure 8. Distribution of hours at various power-output levels as a function of the Wind Farm Wind Factor ϕ_{WF}

The *x* axis is ϕ_{WF}, and the *y* axis denotes the fraction of hours in the year at the indicated power levels. Different color bands represent time spent below power thresholds of 10%, 25%, 50%, 75%, and 100% of rated power. The secondary *x* axis indicates the corresponding wind farm CF, taken as 90% of the theoretical maximum for each ϕ_{WF}.

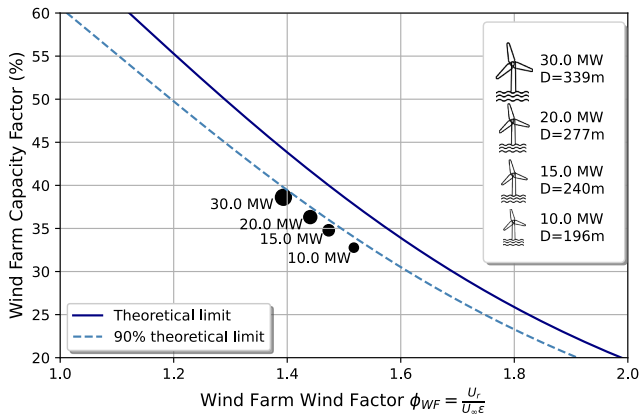

Figure 9. Effect of turbine size (varying rotor diameter and hub height) on the Wind Farm Wind Factor, ϕ_{WF}, and the consequent wind farm capacity factor (%)

The plot shows the theoretical limit (solid line) and 90% of that limit (dashed line). The lowest blade-tip height is 30 m, the rotor specific power is 332 W/m^2, the wind farm size is 10 GW, and the average wind speed at the reference height $h = 150$ m is $U_\infty = 10$ m/s. Wind farm density is 10 MW/km^2 of installed power.

This concentration heightens susceptibility to curtailment, if the grid or storage cannot absorb surpluses during peak episodes. At the same time, more turbines must be installed to reach the same energy target, increasing both total capacity and the risk of oversupply.

As seen in Figures 4 and 5, new high-density offshore projects could realistically yield capacity factors around 30%–40%, well below the 47%–55% range commonly assumed in many integration studies.[3,4,29–31] Consequently, offshore wind's variability profile begins to resemble that of onshore wind from a grid integration perspective, implying that a significant portion of future energy system costs will hinge on these realistic capacity factors.[2]

Impact of turbine size and specific power

In this section, we investigate two key approaches for enhancing offshore wind farm performance: increasing turbine size (i.e., enlarging rotor diameter and raising hub height) and modifying turbine-specific power. These design choices affect the Wind Farm Wind Factor, ϕ_{WF}, through several channels: (1) the rated wind speed, U_r, which is directly influenced by the turbine's specific power; (2) the unperturbed average wind speed at hub height, U_∞, which is linked to the turbine's elevation within the ABL; and (3) the velocity reduction factor, ϵ, which depends on turbine height, spacing, and wind farm layout.

By comparing different rotor diameters, layouts, and specific-power configurations, we demonstrate how design choices aimed at capturing stronger winds aloft or installing more capacity within a given footprint interact with wake dynamics and boundary-layer constraints, ultimately shaping the achievable capacity factor.

Figure 9 illustrates the impact of varying rotor diameter on wind farm performance. As the rotor diameter increases, the rated power of the turbine increases while the specific power (and thus U_r) remains constant. Simultaneously, the increased hub height elevates U_∞ and ϵ, which results in a lower ϕ_{WF} and a higher capacity factor, CF. Our analysis indicates that variations in ϵ have a more pronounced effect on *CF* than changes in U_∞.

Figure 10 presents the effect of varying turbine-specific power (by altering U_r) under two distinct strategies. In the first strategy, turbine spacing is held constant (thereby keeping ϵ constant), while the wind farm's installed capacity density varies. In the second strategy, the wind farm capacity density is maintained constant by varying spacing and therefore ϵ. The average speed of the unperturbed wind at hub height U_∞ remains constant at 10 m/s. The secondary *x* axis in the figure displays the corresponding CF, while the *y* axis represents the power density (i.e., the average power produced per unit area). Marker sizes and transparencies indicate turbine-specific power values ranging from 100 to 500 W/m^2.

The results reveal that for both strategies, power density exhibits an almost linear relationship with the Wind Farm Wind Factor. In the constant-turbine-spacing scenario, achieving higher capacity factors by reducing turbine-specific power is accompanied by a substantial decline in power density, with this decline occurring at a rate that is slightly more than linear in relation to ϕ_{WF}. Conversely, in the constant-capacity-density scenario, attaining both a higher capacity factor and increased power density is feasible only by reducing the spacing between turbines (higher turbine density).

Conclusions

This study establishes a physically grounded upper limit on wind farm performance, demonstrating that aerodynamic constraints impose a fundamental ceiling on the energy extractable from the marine ABL. Central to this finding is the Wind Farm Wind Factor—a dimensionless parameter that concisely captures the

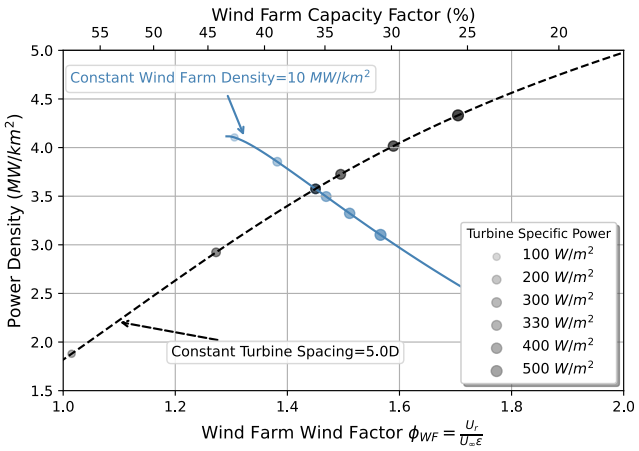

Figure 10. Wind farm power density and capacity factor as functions of the Wind Farm Wind Factor, ϕ_{WF}

The black dashed line corresponds to constant-turbine-spacing (5D), while the blue curve represents the scenario of constant wind farm density (10 MW/km^2). Marker size and transparency denote different turbine-specific power values. In this analysis, the rotor diameter is D = 240 m, the average wind speed at hub height (h = 150 m) is U_∞ = 10 m/s, and the wind farm size is 10 GW.

influence of wind resource, turbine design, and farm layout on achievable capacity factor. The sensitivity to the Weibull shape factor *k* is shown to be comparatively minor.

The Wind Farm Wind Factor provides an elegant and straightforward approach to assessing wind farm performance, requiring only the local wind speed, the rated wind speed of the turbine, and a simplified representation of wind farm layout based on turbine density and frontal distribution. This relationship has been encapsulated in a clear analytical formula.

We validated the developed model extensively using historical operational data from 72 offshore wind farms, collectively representing more than 420 years of production records. The validation results demonstrate excellent agreement with real-world performance data, reflected in a strong correlation between predicted and observed production once operational losses are accounted for.

Leveraging the validated model, we evaluated offshore wind policy targets from several countries, including the UK, France, Germany, the US, the Netherlands, and Belgium. Our analysis identified substantial and systematic discrepancies between national policy projections and the realistic aerodynamic limits. Notably, the Dutch offshore wind program exhibited the most significant overestimation, predicting capacity factors nearly 50% above feasible limits. Similar, although less extreme, overestimations were observed for France (up to 22%), Belgium (24%), and the US (13%–20%). Such widespread discrepancies underscore a global risk of inflated expectations, potentially leading to misguided investments and infrastructure planning and failure of energy supply.

An important additional insight from our analysis is that the most significant reductions in capacity factor occur as wind farm density increases from isolated to moderate levels (i.e., up to 7 MW/km^2). Beyond this, further increases in density result in much smaller incremental losses in capacity factor. Given the limitations of available marine space, very high-density wind farms (i.e., above 15 MW/km^2) may therefore be desirable, despite slightly lower individual turbine efficiency. Although these dense configurations require more materials and pose system integration challenges, their benefits for marine space conservation could justify the trade-off—particularly in crowded or ecologically sensitive environments, where maximizing total yield per unit area must be balanced with the need to protect marine habitats and biodiversity.

These findings strongly indicate that foreseeable offshore wind capacity factors will be substantially lower than values currently assumed in major energy integration and system planning studies. Recognizing and correcting these biases are critical to the integrity and effectiveness of energy policy and infrastructure decisions. The security of energy supply is crucial, and mistakes in long-lead projects are difficult to correct. Systematic overestimation of capacity factor risks not only project underdelivery and financial shortfalls but also threatens energy security, investor confidence, and the credibility of national decarbonization strategies. This model provides a clear benchmark that can be used by system operators, policymakers, planners, and investors to set physically robust expectations and align investments with achievable targets.

Our analytical model helped us to carefully examine how important wind turbine design factors, especially hub height and specific rotor power, affect performance of and energy capture in wind farms. This assessment clarifies which design adjustments yield meaningful improvements in wind farm performance and energy capture.

Although primarily developed for offshore conditions, the proposed model is sufficiently general to be directly applicable to large-scale onshore wind farms as well.

In summary, this study presents and validates a robust, simple, and physically grounded analytical model for wind farm power production. By unifying turbine design, wind resource, and farm layout into a single dimensionless parameter—the Wind Farm Wind Factor (ϕ_{WF})—this work offers both a scientific advance and a practical tool. It clarifies the aerodynamic limits of wind energy while providing planners, policymakers, industry, investors, and civil society with a transparent and reliable benchmark for setting credible, physically achievable expectations. The model's accessibility also empowers non-specialists to independently evaluate proposed projects and challenge unrealistic or unsustainable plans, supporting informed debate on energy security and environmental scrutiny in crowded or ecologically sensitive marine environments.

METHODS

Previous research on limits of offshore wind

Various research studies have attempted to determine how much energy can be extracted from the atmospheric wind system. Depending on diverse assumptions regarding wind classes, capacity factors, available areas, and geographic locations, a wide range of estimates were obtained. In Archer and Jacobson[32] and Marvel et al.,[33] limits to global wind power were investigated using geophysical considerations. In Adams and Keith,[34]

it was shown that previous investigations may have overestimated the available wind power by overlooking large-scale effects of wind turbines on average atmospheric wind speeds. In Enevoldsen et al.,[35] regional socio-technical restrictions and regulations were introduced to assess onshore wind power potential in Europe. In Miller et al.,[36] an analytical approach was proposed to determine the maximum wind power available per unit area, treating the large-scale wind farm as an extra friction source in the ABL. Assuming the rate of momentum generation in the ABL remains unchanged by the wind farm, this additional friction yields a new equilibrium of the momentum equation at lower wind speeds near ground and wind farm heights. This reasoning is similar to that of Frandsen,[13] which uses the geostrophic wind speed as the unperturbed term. The later work by Miller et al.[37] employs a large-scale regional atmospheric weather model with wind turbine parametrization to study global wind limits, further investigating how wind farm density affects the capacity factor—showing substantial efficiency reductions when density (and thus wake interactions) increases. The relationship between wind farm capacity factor and power density was also demonstrated numerically by Pryor et al.[38] for US offshore wind farms, who compared their results with the trends reported in Agora Energiewende et al.[8] for German offshore wind farms. Notably, the results from our analytical model align closely with both the findings of Pryor et al.[38] and Agora Energiewende et al.[8]

The work of Kirby et al.[39] developed a model to estimate the power output along the length of a two-dimensional wind farm by using a boundary-layer approach, in which the evolution of the boundary-layer height governs turbulent entrainment and pressure gradient. This framework considers momentum exchange at two distinct scales: those caused by turbine-wake interactions within the farm and those caused by the interaction of the entire wind farm with the ABL. The analytical model captures the evolution of momentum exchange throughout the depth of the wind farm, providing a practical solution for finite-size farms. It builds directly on the two-scale theory proposed by Nishino and Dunstan.[40] Similarly, Luzzatto-Fegiz and Caulfield[41] adopted a related formulation, providing a more detailed description of the two-dimensional boundary layer, particularly the wake system at the edge of the actuator-disk array representing the turbines, while also incorporating the effects of ABL stability.

Building on these developments, the analysis in Kirby et al.[42] decomposed wind farm performance into the two components of turbine-wake and farm-atmosphere losses and validated this approach against large-eddy simulations of finite-size farms. Their analysis showed that losses from turbine-wake interactions are nearly insensitive to atmospheric conditions, while losses caused by farm-atmosphere interactions depend strongly on boundary-layer stratification but not on turbine layout. For staggered layouts, which are the most common configuration of real wind farms, efficiency losses at the turbine-wake scale were negligible, meaning that the exchange at the turbine-wake scale was rapidly transferred through momentum exchange to the atmospheric scale, where virtually all efficiency reductions were ultimately observed. Even in the less common aligned configuration, the dominant reduction in performance was still due to the farm's impact on the atmosphere. Furthermore, the efficiency associated with atmospheric interaction predicted by their analytical model agreed with simulation results to within about 5%–6%. Their study also demonstrated that the conventional division into wake and blockage losses is not an effective framework for explaining farm performance. This also helps to explain our own policy analysis results in the section on evaluation of national offshore wind policies, where the largest errors were linked to policy/project estimates based on models that emphasized turbine-wake losses while largely ignoring the ABL interaction. Only for some of the study cases was it possible to determine the source for the policy or project estimate; in other cases, values were simply stated in official publications without reference to a methodology.

While the models in Kirby et al.,[39] Nishino and Dunstan,[40] Luzzatto-Fegiz and Caulfield,[41] and Kirby et al[42] largely neglect the properties of the broader atmosphere (such as geostrophic wind speed and Coriolis forces), the work in Antonini and Caldeira[43] explores the opposite end of the spectrum, evaluating the global limits of wind energy extraction by explicitly accounting for Coriolis forces, geostrophic wind speed, and available power density over the globe. From an ABL perspective, the work of Wang et al.[44] provides valuable insights into how clusters of wind farms interact aerodynamically, gradually merging to form a continuous large-scale wind farm system.

The work of Frandsen et al.[45] sought to combine modeling at the intra-wind farm scale (using wake models) with the atmospheric scale, as formulated by Frandsen.[13] In line with these formulations of wind farms within the ABL, the foundational studies by Templin[46] and Newman[47] should also be acknowledged. This progression leads to the models employed in the present study.

Derivation of the theoretical upper limit for the production of a wind farm

The derivation of the theoretical upper limit for the production of a wind farm builds upon the formulation presented by Sørensen and Larsen[14] and Sørensen et al.,[48] based on the wind farm velocity models by Frandsen,[13] Templin,[46] and Emeis and Frandsen.[49] We derive a closed-form expression for the maximum achievable capacity factor by considering (1) the aerodynamic interactions in an infinite wind farm, (2) a simplified power curve, and (3) a two-parameter Weibull distribution for wind speeds. We then extend this derivation to *finite* wind farms.

To arrive at an upper limit, we assume the turbine cut-in wind speed to be $0 m/s$ and the cut-out wind speed to be infinite. This slightly overestimates real production but is consistent with our approach to bounding the maximum capacity factor. With this assumption, we define the power curve P of the wind farm as a function of the wind speed U inside the wind farm at the height of the wind turbine hub, as

$$P(U) = \begin{cases} P_r \left(\frac{U}{U_r}\right)^3 & \text{for } U \leq U_r \\ P_r & \text{for } U_r \leq U \leq +\infty \end{cases} \quad \text{(Equation 1)}$$

Once the rated power P_r and rated wind speed U_r are defined, we need to estimate the wind velocity at hub height inside the wind farm. The presence of the wind farm adds flow resistance

to the lower regime of the ABL, thus changing the velocity profile. The velocity at hub height in the *infinite* wind farm is defined, as derived by Frandsen,[13] Templin,[46] and Frandsen, [50] on the assumption that the wind field inside the wind farm is in equilibrium with the flow field of the ambient ABL. The following is specifically assumed:

- the velocity profile, describing the horizontal mean velocity component within and above the wind farm, is continuous along the height;
- the wind farm is infinite, meaning it is large enough for the vertical wind profile to be horizontally homogeneous;
- the horizontally homogeneous vertical wind profile is logarithmic both below and above hub height (logarithmic wind speed profiles implicitly imply an assumption of neutral ABL stratification);
- the height of the planetary boundary layer is considerably larger than the wind turbine hub height; and
- turbulent wind speed fluctuations are horizontally homogeneous.

Referring to Frandsen[13] and Sørensen and Larsen,[14] the velocity at hub height inside the infinite wind farm is given by

$$U_h = \frac{G}{1+\frac{1}{\kappa}\ln\left(\frac{G}{f'h}\right)\sqrt{c_t+\left(\frac{\kappa}{\ln(h/z_0)}\right)^2}} \quad \text{(Equation 2)}$$

with the wind farm thrust coefficient, c_t, defined as

$$c_t := \frac{\pi}{8}\frac{C_T}{S^2} \quad \text{(Equation 3)}$$

where C_T is the wind turbine thrust coefficient, and S is the average distance between the wind farm turbines measured in turbine diameters (see Sørensen and Larsen[14]).

Equation 2 expresses the wake-reduced wind farm mean wind speed, U_h, at hub height, assuming an equilibrium ABL accounting for the wake effects within an assumed infinite wind farm. This formulation considers the wind speed reduction due to wake effects as a function of c_t, the hub height h, and the geostrophic wind speed, G. In our methodology, the geostrophic wind speed at each wind farm location is inferred from the local unperturbed mean wind speed at hub height U_∞. Specifically, we use the wind profile equation for U_h with the thrust coefficient c_t set to zero (i.e., no wind farm effect), allowing us to solve for G using the site-specific hub height, surface roughness, and latitude. This ensures that the vertical wind profile in the model reflects the actual atmospheric conditions at each location. We assume a logarithmic wind profile, with z_0 being the surface roughness length and κ being the von Kármán constant (typically taken as ≈ 0.4). The geostrophic wind speed is influenced by the Coriolis force, where $f = 2\Omega \sin\theta$ is the Coriolis parameter, in which Ω denotes the rotational speed of the earth, and θ is the latitude. For convenience, we have defined $f' = fe^{A^*}$, in which the constant $A^* = 4$ at latitude 55°. Figures 11 and 12 show graphical representations of the model. For more information, we refer to Frandsen,[13] where the model is described in more detail.

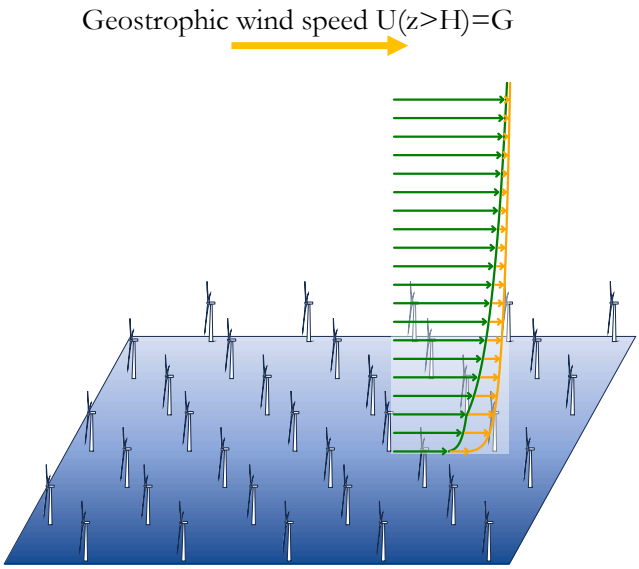

Figure 11. Representation of the velocity profile of the ABL inside the wind farm (green) and in the absence of the wind farm (orange), up to the geostrophic wind speed

Wind resource and production model

To estimate the wind farm power production, we need to model the convolution of the wind speed distribution with the power curve of the wind farm/turbine. We follow the approach presented in Sørensen and Larsen,[14] using a two-parameter Weibull distribution model for the wind speed at a given height.

$$f(x;k,\lambda) = \begin{cases} \frac{k}{\lambda}\left(\frac{x}{\lambda}\right)^{k-1} e^{-\left(\frac{x}{\lambda}\right)^k} & \text{for } x \geq 0, \\ 0 & \text{for } x < 0 \end{cases} \quad \text{(Equation 4)}$$

Equation 4 describes the Weibull probability density function, which is widely used to model wind speed distributions. Here, x represents the wind speed, k is the distribution *shape* parameter, and λ is the distribution *scale* parameter.

The maximum possible yearly energy production $P_{WF,y}$ from an infinite wind farm wind turbine is obtained by convoluting the turbine power curve $P(U)$ over the total range of wind farm wind speeds—thus ignoring both turbine cut-in and cut-out wind speeds—with the Weibull distribution of *wind farm* wind speeds as follows:

$$\begin{aligned} P_{WF,y} &= \int_0^{+\infty} \mathrm{P(U)} f(U;\lambda,k)\mathrm{dU} \\ &= P_r \int_0^{\mathrm{Ur}} \left(\frac{U}{\mathrm{Ur}}\right)^3 f(U;\lambda,k)\mathrm{dU} + Pr \int_{\mathrm{U}}^{+\infty} f(U;\lambda,k)\mathrm{dU} \end{aligned} \quad \text{(Equation 5)}$$

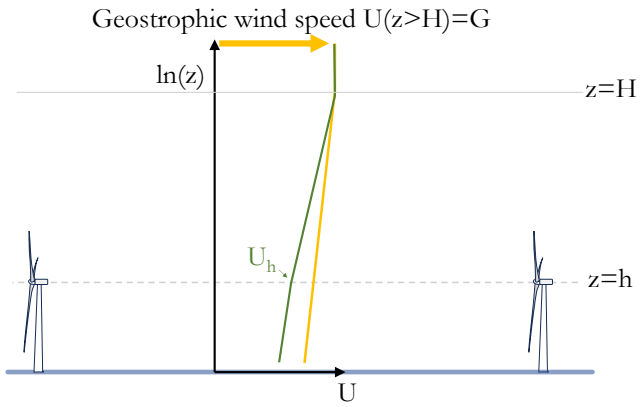

Figure 12. Log-scale representation of the velocity profile of the ABL inside the wind farm (green) and in the absence of the wind farm (orange), up to the geostrophic wind speed
Scales are not proportional.

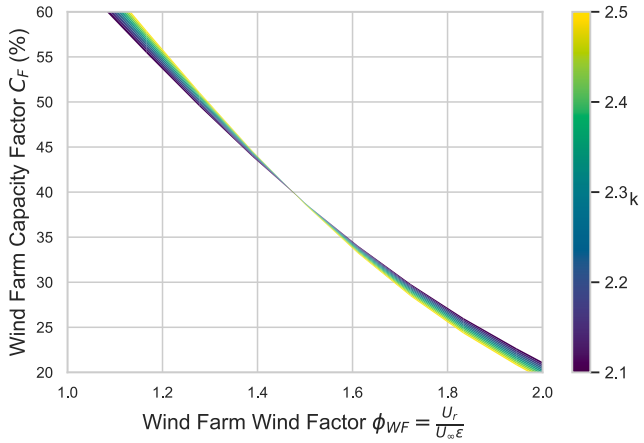

Figure 13. Limit of the capacity factor $C_{F_{max}}$ as a function of Wind Farm Wind Factor $\phi_{WF} = \frac{U_r}{U_\infty \epsilon}$ and the shape factor k of the Weibull distribution of the wind speed (color range)

Equation 6 defines ϵ, which is the ratio between the wind speed in the infinite wind farm and the unperturbed ambient wind speed at hub height, up to rated wind speed. The parameters γ and δ are defined by Equation 7 as follows:

$$\epsilon := \frac{U}{U_\infty} = \frac{1+\frac{\gamma}{\delta}}{1+\frac{\gamma}{\kappa}\sqrt{\frac{\pi C_{T,\text{rated}}}{8S^2}+\left(\frac{\kappa}{\delta}\right)^2}} \quad \text{(Equation 6)}$$

where

$$\gamma := \ln\left(\frac{G}{f'h}\right),\ \delta := \ln\left(\frac{h}{z_0}\right) \quad \text{(Equation 7)}$$

With reference to Sørensen and Larsen[14] and taking the cut-out wind speed as infinity, Equation 5 can finally be written as Equation 8, which gives a closed-form expression for the average annual energy production of Equation 5, using the (lower) incomplete gamma function $\Gamma_{ic}(\star,\star)$:

$$P_{WF,y} = \frac{P_r}{U_r^3}(\epsilon\lambda)^3\Gamma_{ic}\left(\frac{3+k}{k},\left(\frac{U_r}{\epsilon\lambda}\right)^k\right)+P_r e^{-\left(\frac{U_r}{\epsilon\lambda}\right)^k} \quad \text{(Equation 8)}$$

Definition of the Wind Farm Wind Factor. The description of a wind farm is characterized by several variables; some define the shape and dimensions of the wind farm (e.g., spacing between wind turbines), others the local wind resource (e.g., shape and scale factors of the wind speed distribution), others the properties of the wind turbines (e.g., rated wind speed, hub height), and still others the load that the wind farm exerts on the atmosphere. The diverse range of variables makes each wind farm unique. Furthermore, these variables collectively influence the wind farm's capacity factor *CF*, meaning the average power produced over the power installed. Consequently, the problem manifests itself as multi-parametric. However, for simplicity, we aim to transform it into a predominantly *one-parameter* problem, where the capacity factor is principally determined by a single variable. In Equation 8, the key quantity governing the power of the wind farm is the ratio $U_r/(\epsilon\lambda)$. For clarity and practical relevance, we instead express this ratio in terms of the unperturbed mean wind speed at hub height, U_∞, which is directly related to λ through the properties of the Weibull distribution. This choice facilitates interpretation and comparison across different sites and conditions, and it forms the basis for the definition of the Wind Farm Wind Factor used throughout this study. We define this ratio as the *Wind Farm Wind Factor* ϕ_{WF}, expressed by Equation 9:

$$\phi_{WF} := \frac{U_r}{U_\infty \epsilon} \quad \text{(Equation 9)}$$

where U_r is the rated wind speed of the turbine model used in the wind farm; U_∞ is the average speed of the unperturbed wind at the location of the wind farm (in the absence of the wind farm), at hub height. Expressed in terms of the Weibull distribution, it is defined as

$$U_\infty := \lambda\cdot\Gamma\left(\frac{1+k}{k}\right) \quad \text{(Equation 10)}$$

where $\Gamma(\star)$ is the gamma function.

We can define an upper limit for the maximum capacity factor CF_{max} as

$$CF_{max} := \frac{P_{WF,y}}{P_r} = \phi_{WF}^{-3}\Gamma\left(\frac{1+k}{k}\right)^{-3}\Gamma_{ic}\left(\frac{3+k}{k},\phi_{WF}^k\Gamma\left(\frac{1+k}{k}\right)^k\right) + e^{-\phi_{WF}^k\Gamma\left(\frac{1+k}{k}\right)^k} \quad \text{(Equation 11)}$$

Equation 11 shows that the maximum capacity factor is just a function of the Wind Farm Wind Factor and the shape factor of the Weibull distribution. The moderate sensitivity of the maximum capacity factor to the Weibull shape factor is illustrated in Figure 13.

The upper limit capacity factor formulated in Equation 11 relates to an *infinite* wind farm, with ABL flow field being in equilibrium with the wind farm flow field. Real wind farms, however, are *finite* in size,

and turbines at the upwind edges experience less wake interaction and therefore higher wind speeds. This effect is, in Sørensen and Larsen[14] and Sørensen et al.,[51] handled by suitable weighting of production from turbines operating under fully developed wind farm conditions and those operating under unperturbed inflow conditions. Introducing weighting factors w_F and w_S for turbines operating under, respectively, wind farm and solitary conditions, the finite farm upper limit capacity factor can be expressed as

$$CF_{Fmax} = w_F \left[\Phi_{WF}^{-3}\,\Gamma\left(\frac{1+k}{k}\right)^{-3}\Gamma_{ic}\left(\frac{3+k}{k}, \Phi_{WF}^{k}\,\Gamma\left(\frac{1+k}{k}\right)^{k}\right) + e^{-\Phi_{WF}^{k}\,\Gamma\left(\frac{1+k}{k}\right)^{k}} \right] + w_S \left[\left(\frac{U_r}{U_\infty}\right)^{-3}\Gamma\left(\frac{1+k}{k}\right)^{-3} \Gamma_{ic}\left(\frac{3+k}{k}, \left(\frac{U_r}{U_\infty}\right)^{k}\Gamma\left(\frac{1+k}{k}\right)^{k}\right) + e^{-\left(\frac{U_r}{U_\infty}\right)^{k}\Gamma\left(\frac{1+k}{k}\right)^{k}} \right] \quad \text{(Equation 12)}$$

which can be recast as

$$CF_{F_{max}} = w_F \left[\Phi_{WF}^{-3}\,\Gamma\left(\frac{1+k}{k}\right)^{-3}\Gamma_{ic}\left(\frac{3+k}{k}, \Phi_{WF}^{k}\Gamma\left(\frac{1+k}{k}\right)^{k}\right) + e^{-\Phi_{WF}^{k}\Gamma\left(\frac{1+k}{k}\right)^{k}} \right] + w_S \left[\frac{\lambda^3}{U_r^3}\,\Gamma_{ic}\left(\frac{3+k}{k}, \left(\frac{U_r}{\lambda}\right)^{k}\right) + e^{-\left(\frac{U_r}{\lambda}\right)^{k}} \right] \quad \text{(Equation 13)}$$

where the weighting factors are defined by, respectively

$$w_F := 1 - \frac{a}{\sqrt{N_T}} \text{ and } w_S := \frac{a}{\sqrt{N_T}} \quad \text{(Equation 14)}$$

with N_T being the number of wind farm turbines, and $a = 5.3$[51] (in Sorensen and Larsen[14] $a = 3$). Figure 14 illustrates the effect of the weighting factors.

These weighting factors are based on the assumption of a squared wind farm layout and uniform wind direction, providing a general estimate for the proportion of edge versus interior turbines (an illustration of the power distribution within squared wind farms can also be found in Wu et al.[52]).

However, for the wind farms in our validation database and case studies, we refined this approach; rather than applying a fixed formula, we considered each wind farm's specific layout, including aspect ratio, dominant wind direction, and the influence of neighboring wind farms, to determine the number of turbines experiencing unperturbed inflow. In practice, this meant defining the edge region as a context-dependent number of rows or turbines at the perimeter. This individualized method allows for a more realistic assignment of edge and interior turbines, thereby improving the fidelity of our performance predictions. The resulting values for each wind farm are provided in Simão Ferreira.[15] It should be noted that for very large wind farms, even turbines at the upwind edge may experience some reduction in wind speed due to farm-scale induction effects; however, this effect is typically small compared with the wake and layout influences already accounted for in our model, and it is therefore neglected for simplicity.

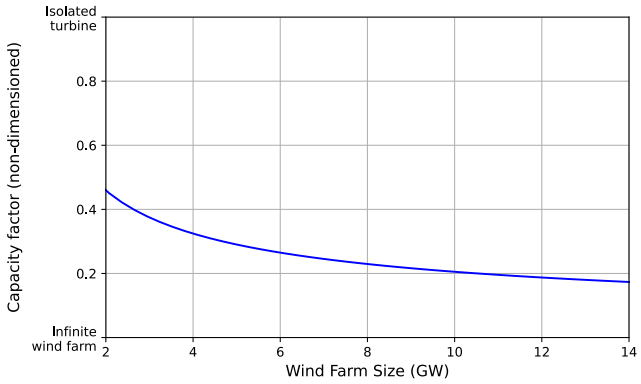

Figure 14. Effect of wind farm size on non-dimensional CF, based on Equations 13 and 14

The wind farm size is expressed in GW, assuming a turbine rating of 15 MW. As wind farm size increases, the proportion of turbines operating under unperturbed (edge) conditions decreases, and the average capacity factor approaches the limit for an infinite wind farm. The upper left tends to be isolated turbine conditions, while the lower right approaches the fully developed wake regime of a very large farm.

An equivalent Finite Wind Farm Wind Factor ϕ_{FF} for the finite-size wind farm can be defined as

$$\phi_{FF} := \frac{U_r}{U_\infty \epsilon_{eq}} \quad \text{(Equation 15)}$$

where ϵ_{eq} denotes the equivalent finite wind farm value of the infinite farm velocity reduction factor ϵ. Using Equation 13, ϕ_{FF} is obtained from numerically solving the transcendental Equation 16

$$\Phi_{FF}^{-3}\,\Gamma\left(\frac{1+k}{k}\right)^{-3}\Gamma_{ic}\left(\frac{3+k}{k}, \Phi_{FF}^{k}\Gamma\left(\frac{1+k}{k}\right)^{k}\right) + e^{-\Phi_{FF}^{k}\Gamma\left(\frac{1+k}{k}\right)^{k}} = w_F \left[\Phi_{WF}^{-3}\Gamma\left(\frac{1+k}{k}\right)^{-3}\Gamma_{ic}\left(\frac{3+k}{k}, \Phi_{WF}^{k}\Gamma\left(\frac{1+k}{k}\right)^{k}\right) + e^{-\Phi_{WF}^{k}\Gamma\left(\frac{1+k}{k}\right)^{k}} \right] + w_S \left[\frac{\lambda^3}{U_r^3}\,\Gamma_{ic}\left(\frac{3+k}{k}, \left(\frac{U_r}{\lambda}\right)^{k}\right) + e^{-\left(\frac{U_r}{\lambda}\right)^{k}} \right] \quad \text{(Equation 16)}$$

from which the equivalent finite wind farm velocity reduction factor, ϵ_{eq}, readily follows from Equation 15.

Wind farm data collection

Wind farm data for this study were collected from a variety of public, verifiable sources to ensure a comprehensive dataset that covers 72 offshore wind farms, represented by 71 data points (the two Trianel wind farms are analyzed as one data point in the present study, due to their combined layout), and that uses over 420 years of data in total. The dataset is publicly available and can be accessed in Simão Ferreira.[15] Data for each wind farm were collected from multiple platforms, including industry reports, renewable energy databases, government and regulator publications, and study reports (see, e.g., Borrmann,[53] Belgian Offshore Platform,[54] Vattenfall,[55] and Nordsee One GmbH[56]). The data sources for the estimation of the wind farm capacity factor, including the years considered, are also presented in Simão Ferreira.[15]

For wind farms equipped with more than one turbine model, we derive an equivalent rotor diameter using a capacity-weighted average of the specific power of the turbines. This ensures that each wind farm can be described by an ''equivalent'' turbine rating and rotor size. The location of the wind farms is shown in Figure 1. Figure 2 shows the distribution of the wind farm size in MW and the wind farm density in MW/km^2 of the dataset, where the marker size is proportional to the rotor size, and lists the wind farms as described in Simão Ferreira.[15]

The wind farms included in our validation dataset were selected based on the availability of public data, specifically requiring complete annual production records and information required for the model. Of the 72 wind farms in the dataset, only 5 have fewer than 30 turbines, ensuring that the sample is representative of small-scale to large-scale, commercial offshore wind projects. This selection minimizes potential biases associated with very small demonstration or pilot-scale wind farms.

We collected several key parameters for each farm, including total installed capacity (in megawatts, MW), the area covered by the wind farm (in square kilometers, km^2), the number of wind turbines, the rated power of each turbine (in MW), the diameter of the rotor D (in meters, m), and the height of the nacelle h (m). For each wind farm location, the average annual unperturbed ambient wind speed at a given reference height (h_w) was recovered from Technical University of Denmark.[21] The wind speed distribution is assumed to follow a Weibull distribution, with the shape parameter k = 2.4 considered to be representative for all locations.[48] With this assumption, we determine the scale parameter λ for each location from the annual mean wind speed. The simulations assume a surface roughness $z_0 = 10^{-4}m$, which is considered representative for offshore conditions.[48] The power coefficient and thrust coefficient at wind speeds below rated are assumed to be the same for all turbines $C_P = 0.46$ and $C_T = 0.75$.

While the dataset used for model validation is geographically focused on the Baltic, North, and Irish Seas, the underlying physical principles and validation results are broadly applicable to offshore wind farms in other regions. Some variations may occur in wind farms situated in areas with strongly accelerated flows, such as those influenced by complex coastal or island topography. Furthermore, the variation of the geostrophic drag law with respect to latitude has been examined in previous studies, e.g., Antonini and Caldeira.[43]

Descriptions of case studies of policy goals

In addition to validating our model with historical wind farm data, in the section on evaluation of national offshore wind policies, we examine large-scale offshore wind projects and national policy targets (summarized in Table 1) to evaluate how their planned capacity factors compare against our theoretical limit. Here, we provide further details on these planned offshore wind developments. Specifically, we describe the site locations, the assumed turbine sizes and ratings, and the overall project layouts adopted in our simulations.

UK

This case study is based on the planned Hornsea 3 wind farm in the North Sea (53.8°N, 2.5°E), intended to expand the UK's offshore wind capacity. Current publicly available descriptions indicate a project range of around 211–231 turbines, each assumed to be rated at 14 MW with a 236-m rotor diameter. For the simulations in this study, we considered 211 turbines (14 MW, D = 236 m), yielding a total installed capacity of 2,955 MW across 696 km^2, corresponding to 4.25 MW/km^2.[57–60]

FR 1

This case study examines the planned Centre Manche wind farms (I and II) in the Channel region of France (49.9°N, 0.7°W). Public project outlines describe approximately 107 turbines, each assumed to be rated at 23.3 MW with a 300-m rotor diameter. For our modeling, we use these nominal values to represent a total of 2,497 MW across 453 km^2, achieving 5.51 MW/km^2.[61–66]

FR 2

Based on early planning for Oléron I (45.8°N, 1.8°W) off France's Atlantic coast, projections suggest around 51 turbines, nominally 23.3 MW each with a 300-m rotor diameter. We adopt these figures in our simulations, giving a total of 1,200 MW over 180 km^2 corresponding to 6.67 MW/km^2.[61,67,68]

DE 1

For the German North Sea (56.0°N, 6.3°E), the planned N11–13 wind farm areas might ultimately feature a range of turbine numbers and sizes. We model a scenario of 545 turbines at 22 MW, 290-m rotors for a total of 12,000 MW over 1,157 km^2, resulting in 10.37 MW/km^2.[69–73] Proposed N-12.4-.5 extensions[74–77] (an additional 4,000 MW) lie outside our study scope and would further reduce capacity factors.[77]

DE 2

Similarly, the N9 area (54.5°N, 5.8°E) in the German North Sea is projected to have about 367 turbines. For this analysis, we use 15-MW rated turbines with a 240-m rotor, totaling 5,500 MW across 421 km^2 (13.06 MW/km^2).[69–73] Extensions N-9.4-.5[74–77] (2,000 MW) east of N9 are excluded but would diminish capacity factors further.[77] The analysis in Vollmer and Dörenkämper[78] applies an updated version of their model (see Vollmer et al.[79]), yielding alternative energy production estimates about 6%–8% higher. While these revised results align more closely with our model predictions, in this study, we rely on the earlier outcomes of Vollmer and Dörenkämper,[69] since the approach in Vollmer

et al.[79] has so far only been validated at the single-turbine scale. This is also true for study case *DE 1*.

US 1

The Atlantic Shores South zone, off New Jersey (39.3°N, 74.1°W), is our first US case study. We simulate 189 turbines at 15 MW with 236-m-diameter rotors, giving 2,836.6 MW across 413.3 km^2 (6.86 MW/km^2).[80–85]

US 2

The New York Bight (39.53°N, 73.32°W) offshore region is slated for multiple wind projects, including Atlantic Shores Offshore Wind Bight, Leading Light Wind, Community Offshore Wind, and Attentive Energy.[28,83–86] Current plans suggest roughly 643 turbines at 15 MW each and 236-m-diameter rotors, delivering 9,646 MW over 1,413 km^2 (6.82 MW/km^2), a scenario we adopt in our simulations.

NL

The Dutch North Sea Program (53.3°N, 5.8°E) calls for various possible layouts; our study adopts 667 turbines at 15 MW, each with a 240-m rotor diameter. This leads to a total of 10,000 MW on 1,000 km^2, or 10 MW/km^2.[19,24–27] For the Netherlands, our analysis is based on spatial planning data and power density assumptions from the original North Sea Programme 2022–2027 and the corresponding wind energy infrastructure planning prior to July 2025. In July 2025, the Dutch government published an updated Windenergie Infrastructuurplan Noordzee and an accompanying letter to parliament, revising national targets and providing a more adaptive, phased approach to future offshore wind roll-out.[22,23] The updated plan reflects more realistic projections for supply chain constraints, and ecological limits, and increases the official reference power density for future area calculations to 10.5 MW/km^2; however, it projects higher capacity factors than the original North Sea Programme 2022–2027. For consistency and since the July 2025 update raises assumptions to levels even further beyond theoretical limits, we use the values for the power density and capacity factor from the original North Sea Programme 2022–2027 (pre-July 2025) as our benchmark.

BE

Finally, the Princess Elisabeth Zone in the Belgian North Sea (51.6°N, 2.6°E) is planned to comprise about 219 turbines rated at 16 MW each, with 243-m-diameter rotors, for a total of 3,500 MW over 255.8 km^2. We use these values in our simulations, yielding 13.68 MW/km^2.[87–89]

LCOE estimation methodology

As discussed in the section on impact on cost of energy (see also Figure 6), the LCOE provides a convenient metric for assessing the economic feasibility of offshore wind farms, particularly when evaluating how errors in capacity factor estimates affect overall project costs. Formally, the LCOE is given by:

$$\mathrm{LCOE} = \frac{\text{Total Cost}}{\text{Energy Output}} \qquad \text{(Equation 17)}$$

which can be approximated as inversely proportional to the wind farm capacity factor under the assumption that other cost components remain constant.

However, establishing a precise reference LCOE as a function of capacity factor is challenging, because bottom-fixed offshore wind farm costs vary significantly due to factors such as water depth, distance to shore, supply chain logistics, and cost of capital. After a period of steady decline until around 2018–2019, offshore wind costs have reportedly seen a 30%–60% increase over the past 4 years.[6,7] Furthermore, published LCOE estimates for offshore projects can differ widely, even within the same regions and time frames.[6,10,20,90–104]

By way of illustration, Lazard[10] estimates an LCOE of 75–139 USD/MWh for CF of 45%–55% in US waters, while Stehly et al.[96] reports an average of 117 USD/MWh in 2023 for a 49% capacity factor. The same reference [96] projects a lowest LCOE of 129 USD/MWh by 2025 for the North-Central Atlantic coast at 48% capacity factor. Similarly, Kost et al.[99] finds 55–103 €/MWh in the German North Sea for CF of 37%–51%. On a global scale, DNV[6] reports 133 USD/MWh in 2023, whereas the International Renewable Energy Agency[102] estimates 75 USD/MWh for the same year. In short, definitive consensus on current offshore wind costs remains elusive.

To enable straightforward comparisons within our study, we adopt a reference LCOE of 80 €/MWh at a 50% capacity factor. Recognizing that this figure lies toward the lower end of the documented ranges, we treat it as a baseline. The capacity factor sensitivity is then modeled as

$$\mathrm{LCOE}(CF) = 80 \times \frac{50\%}{CF}\ (€/\mathrm{MWh}). \qquad \text{(Equation 18)}$$

This simplified proportional model allows us to compare different national policy targets and theoretical wind energy limits (section on impact on cost of energy; Figure 6), while acknowledging that real-world LCOE can vary substantially from site to site.

RESOURCE AVAILABILITY

Lead contact

Requests for further information and resources should be directed to and will be fulfilled by the lead contact, Carlos Simão Ferreira (c.j.simaoferreira@tudelft.nl).

Materials availability

This study did not use materials or generate new unique reagents.

Data and code availability

All data used for validation and analysis in this study are publicly available. The offshore wind farm production database employed here is archived in a public repository (Simão Ferreira[15] in the references) and can be accessed and reused under the terms specified therein. All other data used or discussed in this paper are also publicly available as detailed in the references. Table S1 contains a table with the results in Figures 2, 3, and 4.

ACKNOWLEDGMENTS

The authors thank the reviewers and editors for their detailed and constructive feedback, which significantly improved the clarity and impact of this manuscript.

This research did not receive direct sponsorship by any external funding. However, C.S.F. acknowledges support from the X-ROTOR project (Horizon 2020, grant agreement no. 101007135), and J.N.S. acknowledges support from the MERIDIONAL project (Horizon Europe, grant agreement no.

101084216) for dissemination of key results of this work at conferences and project meetings. Additionally, the work in Sørensen[51] (see methods) was partially funded by MERIDIONAL.

C.S.F. also gratefully acknowledges valuable feedback received during presentations and discussions at the Dutch offshore wind innovation consortium GROW (Growth through Research, development & demonstration in Offshore Wind), the Netherlands Enterprise Agency (Rijksdienst voor Ondernemend Nederland, RVO), Rijkswaterstaat, and Eneco.

C.S.F. would also like to thank Eize de Vries (Windpower Monthly) for his early and thoughtful coverage of this research and for facilitating connections with industrial partners, which allowed for informal feedback from industry stakeholders.

Any opinions, findings, and conclusions or recommendations expressed in this material are those of the authors and do not necessarily reflect the views of the supporting organizations.

AUTHOR CONTRIBUTIONS

The three authors defined the overall aim and structure of the paper. G.C.L. and J.N.S. originally developed and published in Sørensen and Larsen[14] the core methodology underlying Equations 1, 2, 3, 4, 5, 6, and 7, along with an initial, more general form of Equation 8. C.S.F. simplified the general form into the infinite wind range case for the final version of Equation 8 to identify the "Wind Farm Wind Factor" and derived the wind farm capacity factor limit as a function of this factor, demonstrating low sensitivity to the Weibull shape parameter *k*. C.S.F. then validated the new formulation against the wind farm database. C.S.F., G.C.L., and J.N.S. jointly developed the final formulation in Equations 11, 12, and 13. G.C.L. and J.N.S. provided the foundational code from Sørensen and Larsen,[14] which C.S.F. adapted for the calculations in this paper. C.S.F. carried out the data collection for the wind farm database and the national policy case studies. All calculations and figures were created and most of the manuscript writing was done by C.S.F., with G.C.L. and J.N.S. co-writing, reviewing, refining, and co-authoring throughout.

DECLARATION OF INTERESTS

The authors declare no competing interests.

DECLARATION OF GENERATIVE AI AND AI-ASSISTED TECHNOLOGIES IN THE WRITING PROCESS

During the preparation of this work, the authors used ChatGPT (OpenAI) to improve the clarity and readability of the manuscript. After using this tool, the authors reviewed and edited the content as needed and take full responsibility for the content of the publication.

SUPPLEMENTAL INFORMATION

Supplemental information can be found online at https://doi.org/10.1016/j.crsus.2025.100573.

Received: August 5, 2025
Revised: September 21, 2025
Accepted: October 28, 2025
Published: November 24, 2025

REFERENCES

1. DNV. (2021). Ocean's future to 2050—a sectoral and regional forecast of the blue economy. Tech. Rep. DNV Høvik, Norway. https://www.dnv.com/oceansfuture/DNV.
2. Gøtske, E.K., Andresen, G.B., Neumann, F., and Victoria, M. (2024). Designing a sector-coupled european energy system robust to 60 years of historical weather data. Nat. Commun. *15*, 10680. https://doi.org/10.1038/s41467-024-54853-3.
3. Kuwahata, R., Copier, J.J., and Hevia-Koch, P. (2024). Integrating solar and wind: Global experience and emerging challenges. Tech. Rep. (International Energy Agency [IEA]) https://iea.blob.core.windows.net/assets/4e495603-7d8b-4f8b-8b60-896a5936a31d/IntegratingSolarandWind.pdf
4. Gonzalez-Aparicio, I., Vitulli, A., Krishna-Swamy, S., Hernandez-Serna, R., Jansen, N., and Verstraten, P. (2022). Offshore wind business feasibility in a flexible and electrified dutch energy market by 2030. Technical Report (TNO). https://publications.tno.nl/publication/34640203/tMITI0/TNO-2022-offshorewind.pdf.
5. DNV. (2024). Offshore wind: The power to progress. Tech. Rep. DNV Høvik, Norway. https://brandcentral.dnv.com/original/gallery/10651/files/original/9478f9fc-86ba-45b7-94d6-38f1d29d4af9.pdf.
6. DNV. (2024). Energy transition outlook 2024: A global and regional forecast to 2050. Tech. Rep. DNV Høvik, Norway. https://www.dnv.com/eto.
7. Weiss, A., Schlosser, A., Kühn, F., Zivansky, J., Aanstad, K.M., and Akersveen, S. (2024). Offshore wind: Strategies for uncertain times (McKinsey Company). https://www.mckinsey.com/industries/electric-power-and-natural-gas/our-insights/offshore-wind-strategies-for-uncertain-times.
8. Agora Energiewende, Agora Verkehrswende, Technical University of Denmark, and Max-Planck-Institute for Biogeochemistry. (2020). Making the most of offshore wind: Re-evaluating the potential of offshore wind in the german north sea. Study commissioned by Agora Energiewende and Agora Verkehrswende. https://www.agora-energiewende.org/publications/making-the-most-of-offshore-wind.
9. McCoy, A., Musial, W., Hammond, R., Hernando, D.M., Duffy, P., Beiter, P., Pérez, P., Baranowski, R., Reber, G., and Spitsen, P. (2024). Offshore wind market report: 2024 edition. Tech. Rep. NREL/TP-5000-90525 (National Renewable Energy Laboratory [NREL] Golden, CO). https://www.nrel.gov/docs/fy24osti/90525.pdf.
10. Lazard. (2024). Lazard's levelized cost of energy+ – version 17.0. Tech. Rep. https://www.lazard.com/media/xemfey0k/lazards-lcoeplus-june-2024-_vf.pdf.
11. Timmer, E. (2024). Offshore wind business feasibility in a flexible and electrified dutch energy market by 2030. Tech. Rep. (TNO) https://www.hhwe.eu/download/netherlands-tno-offshore-wind-business-feasibility-in-a-flexible-and-electrified-dutch-energy-market-by-2030-11-2022/HHWE
12. Stead, S., Tarasewicz, L., and Husband, S.; AFRY Management Consulting (2020). The business case and supporting interventions for dutch offshore wind. Tech. Rep. (AFRY Management Consulting Oxford) https://afry.com/sites/default/files/2020-03/dutch_offshorebusinesscases_onlineversion_final.pdf
13. Frandsen, S. (2007). Turbulence and turbulence-generated structural loading in wind turbine clusters. PhD thesis. https://orbit.dtu.dk/en/publications/turbulence-and-turbulence-generated-structural-loading-in-wind-tu.
14. Sørensen, J.N., and Larsen, G.C. (2021). A Minimalistic Prediction Model to Determine Energy Production and Costs of Offshore Wind Farms. Energies *14*, 448. https://doi.org/10.3390/en14020448.
15. Simao Ferreira, C. (2024). Offshore wind farm energy production database. 4TU.ResearchData. https://doi.org/10.4121/ff8c99b5-c273-4ae0-9c82-4ade1391813a.v1.
16. European Marine Observation and Data Network (EMODnet). (2024). Emodnet geoviewer. https://emodnet.ec.europa.eu/geoviewer/.
17. 4C Offshore. (2024). Offshore wind farms map. https://map.4coffshore.com/offshorewind/.
18. Mortensen, N.G. (2015). 46200 Planning and Development of Wind Farms: Wind resource assessment using the WAsP software (DTU Wind Energy). https://backend.orbit.dtu.dk/ws/portalfiles/portal/118979792/Wind_resource_assessment_using_the_WAsP_software_Report_E_70_ed_2_.pdf.

19. Maassen van den Brink, I., Olijve, N., Pustjens, W., de Sonneville, B., and Geujen, S. (2020). Determination of the cost levels of wind farms (and their grid connections) in new offshore wind energy search areas. Tech. Rep. (BLIX Consultancy BV) https://www.noordzeeloket.nl/publish/pages/194418/determination-of-the-cost-levels-of-wind-farms-and-their-grid-connections-in-new-offshore-wind-energ.pdf

20. Fuchs, R., Zuckerman, G., Duffy, P., Shields, M., Musial, W., Beiter, P., Cooperman, A., and Bredenkamp, S. (2024). The cost of offshore wind energy in the United States from 2025 to 2050. Technical Report NREL/TP–5000-88988 (National Renewable Energy Laboratory [NREL]). https://www.osti.gov/servlets/purl/2433785/.

21. Technical University of Denmark. (2024). Global wind atlas. https://globalwindatlas.info/en.

22. Hermans, S. (2025). Kamerbrief het windenergie infrastructuurplan noordzee. https://www.rijksoverheid.nl/documenten/kamerstukken/2025/07/16/kamerbrief-het-windenergie-infrastructuurplan-noordzee.

23. Ministerie van Economische Zaken en Klimaat. (2025). Het windenergie infrastructuurplan noordzee. Rapport Ministerie van Economische Zaken en Klimaat. https://www.rijksoverheid.nl/documenten/rapporten/2025/07/16/het-windenergie-infrastructuurplan-noordzee.

24. Government of the Netherlands, and Ministry of Infrastructure and Water Management. (2022). North Sea Programme 2022–2027. Tech. Rep. https://www.noordzeeloket.nl/en/policy/north-sea-programme-2022-2027/.

25. Government of the Netherlands (2021). Additional draft north sea programme 2022–2027 (Ministry of Infrastructure and Water Management, Ministry of Agriculture, Nature and Food Safety, Ministry of Economic Affairs and Climate Policy, Ministry of the Interior and Kingdom Relations). https://www.noordzeeloket.nl/publish/pages/197401/additional-draft-north-sea-programme-2022-2027.pdf.

26. Government of the Netherlands (2024). Energie infrastructuur plan noordzee 2050 (Government of the Netherlands). https://www.rijksoverheid.nl/documenten/kamerstukken/2024/06/06/energie-infrastructuur-plan-noordzee-2050.

27. Minister Jetten (Klimaat en Energie) (2024). Kamerbrief over de visie van het kabinet op de verdere realisatie van windenergie op zee na 2030 (Government of the Netherlands). https://open.overheid.nl/documenten/ronl-b34f5ea2f405a4b9dbdfe676288ace0736599264/pdf.

28. Bureau of Ocean Energy Management. (2024). New york bight. https://www.boem.gov/renewable-energy/state-activities/new-york-bight.

29. ENTSO-E, and ENTSOG. (2025). TYNDP 2024 final scenarios report. Tech. Rep. https://2024.entsos-tyndp-scenarios.eu/.

30. International Energy Agency (2024). Managing the seasonal variability of electricity demand and supply. Tech. Rep. (International Energy Agency) https://www.iea.org/reports/managing-the-seasonal-variability-of-electricity-demand-and-supply

31. International; Renewable; Energy Agency (IRENA) (2019). Future of wind: Deployment, investment, technology, grid integration and socio-economic aspects. Tech. Rep. (International Renewable Energy Agency) https://www.irena.org/-/media/Files/IRENA/Agency/Publication/2019/Oct/IRENA_Future_of_wind_2019.pdf

32. Archer, C.L., and Jacobson, M.Z. (2005). Evaluation of global wind power. J. Geophys. Res. *110*, D12110. https://doi.org/10.1029/2004JD005462.

33. Marvel, K., Kravitz, B., and Caldeira, K. (2013). Geophysical limits to global wind power. Nat. Clim. Change *3*, 118–121. https://doi.org/10.1038/nclimate1683.

34. Adams, A.S., and Keith, D.W. (2013). Are global wind power resource estimates overstated? Environ. Res. Lett. *8*, 015021. https://doi.org/10.1088/1748-9326/8/1/015021.

35. Enevoldsen, P., Permien, F.H., Bakhtaoui, I., von Krauland, A.K., Jacobson, M.Z., Xydis, G., Sovacool, B.K., Valentine, S.V., Luecht, D., and Oxley, G. (2019). How much wind power potential does europe have? examining european wind power potential with an enhanced socio-technical atlas. Energy Policy *132*, 1092–1100. https://www.sciencedirect.com/science/article/pii/S0301421519304343.

36. Miller, L.M., Gans, F., and Kleidon, A. (2011). Estimating maximum global land surface wind power extractability and associated climatic consequences. Earth Syst. Dyn. *2*, 1–12. https://esd.copernicus.org/articles/2/1/2011/.

37. Miller, L.M., Brunsell, N.A., Mechem, D.B., Gans, F., Monaghan, A.J., Vautard, R., Keith, D.W., and Kleidon, A. (2015). Two methods for estimating limits to large-scale wind power generation. Proc. Natl. Acad. Sci. USA *112*, 11169–11174. https://pnas.org/doi/full/10.1073/pnas.1408251112.

38. Pryor, S.C., Barthelmie, R.J., and Shepherd, T.J. (2021). Wind power production from very large offshore wind farms. Joule *5*, 2663–2686. https://doi.org/10.1016/j.joule.2021.09.002.

39. Kirby, A., Dunstan, T.D., and Nishino, T. (2023). An analytical model of momentum availability for predicting large wind farm power. J. Fluid Mech. *976*, A24. https://www.cambridge.org/core/journals/journal-of-fluid-mechanics/article/an-analytical-model-of-momentum-availability-for-predicting-large-wind-farm-power/E3F08A6569CB09CCFA8F7D5686982772.

40. Nishino, T., and Dunstan, T.D. (2020). Two-scale momentum theory for time-dependent modelling of large wind farms. J. Fluid Mech. *894*, A2. https://doi.org/10.1017/jfm.2020.252.

41. Luzzatto-Fegiz, P., and Caulfield, C.P. (2018). Entrainment model for fully-developed wind farms: Effects of atmospheric stability and an ideal limit for wind farm performance. Phys. Rev. Fluids *3*, 093802. https://doi.org/10.1103/PhysRevFluids.3.093802.

42. Kirby, A., Nishino, T., Lanzilao, L., Dunstan, T.D., and Meyers, J. (2025). Turbine- and farm-scale power losses in wind farms: an alternative to wake and farm blockage losses. Wind Energy Sci. *10*, 435–450. https://wes.copernicus.org/articles/10/435/2025/.

43. Antonini, E.G.A., and Caldeira, K. (2021). Atmospheric pressure gradients and coriolis forces provide geophysical limits to power density of large wind farms. Appl. Energy *281*, 116048. https://www.sciencedirect.com/science/article/pii/S0306261920314835.

44. Wang, Q., Luo, K., Wu, C., Tan, J., He, R., Ye, S., and Fan, J. (2023). Inter-farm cluster interaction of the operational and planned offshore wind power base. J. Cleaner Prod. *396*, 136529. https://www.sciencedirect.com/science/article/pii/S095965262300687X.

45. Frandsen, S., Barthelmie, R., Pryor, S., Rathmann, O., Larsen, S., Højstrup, J., and Thøgersen, M. (2006). Analytical modelling of wind speed deficit in large offshore wind farms. Wind Energy *9*, 39–53. https://doi.org/10.1002/we.189.

46. Templin, R.J. (1974). An estimate of the interaction of windmills in widespread arrays. Tech. Rep. (National Aeronautical Establishment) https://nrc-publications.canada.ca/eng/view/object/?id=94d3fbff-cb95-4967-8926-ebb4494d1578

47. Newman, B.G. (1977). The spacing of wind turbines in large arrays. Energy Convers. *16*, 169–171. https://www.sciencedirect.com/science/article/pii/0013748077900249.

48. Sørensen, J.N., Larsen, G.C., and Cazin-Bourguignon, A. (2021). Production and Cost Assessment of Offshore Wind Power in the North Sea. J. Phys.: Conf. S. *1934*, 012019. https://iopscience.iop.org/article/10.1088/1742-6596/1934/1/012019.

49. Emeis, S., and Frandsen, S. (1993). Reduction of horizontal wind speed in a boundary layer with obstacles. Boundary-Layer Meteorol. *64*, 297–305. https://doi.org/10.1007/BF00708968.

50. Frandsen, S. (1992). On the wind speed reduction in the center of large clusters of wind turbines. J. Wind Eng. Ind. Aerodyn. *39*, 251–265. https://www.sciencedirect.com/science/article/pii/016761059290551K.

51. Sørensen, J.N., Garcia, A.M.I., Larsen, G.C., Pedersen, M.M., and Fournely, D. (2024). Extension and validation of minimalistic prediction model to determine the energy production of offshore wind farms. J. Phys.:

Conf. S. *2767*, 092022. https://doi.org/10.1088/1742-6596/2767/9/092022.

52. Wu, C., Wang, Q., Luo, K., and Fan, J. (2022). Mesoscale impact of the sea surface on the performance of offshore wind farms. J. Cleaner Prod. *372*, 133741. https://doi.org/10.1016/j.jclepro.2022.133741.
53. Borrmann, R., Rehfeldt, K., Wallasch, A.K., and Lüers, S. (2018). Capacity densities of european offshore wind farms. https://vasab.org/wp-content/uploads/2018/06/BalticLINes_CapacityDensityStudy_June2018-1.pdf.
54. Belgian Offshore Platform. (2020). Offshore wind farm projects in belgium. https://www.belgianoffshoreplatform.be/en/projects/.
55. Vattenfall. (2024). Sandbank power plant. https://powerplants.vattenfall.com/sandbank/.
56. Nordsee One GmbH. (2024). Nordsee one offshore wind farm. https://www.nordseeone.com/.
57. The Crown Estate. (2023). Offshore wind report 2023. https://www.thecrownestate.co.uk/our-business/marine/offshore-wind-report-2023.
58. Ørsted. (2024). About Ørsted. https://orsted.co.uk/about-us/our-company.
59. Ørsted. (2024). Hornsea 3: About the project. https://hornseaproject3.co.uk/about-the-project.
60. Ørsted. (2024). Ørsted in the uk. https://orsted.co.uk/about-us/our-company/in-the-uk.
61. Commission de Régulation de l'Énergie (CRE). (2024). Délibération n°2024-154 du 29 août 2024 portant avis sur les cahiers des charges des procédures ao7 (sud-atlantique / Île d'oléron) et ao8 (centre manche 2). https://www.cre.fr/fileadmin/Documents/Deliberations/2024/240829_2024-154_Avis_CDC_AO7_AO8.pdf.
62. RWE. (2024). Centre manche 2 (ao8) — rwe in france. https://fr.rwe.com/en/our-energy/offshore-wind/our-activities-in-france/centre-manche-2-ao8/.
63. Eoliennes en Mer. (2024). Centre manche 2 – projet centre manche. https://www.eoliennesenmer.fr/facades-maritimes-en-france/facade-manche-mer-du-nord/projet-centre-manche/centre-manche-2.
64. Commission de Régulation de l'Énergie (CRE). (2023). Rapport de synthèse (version publique): Procédure de mise en concurrence avec dialogue concurrentiel n°1/2020 portant sur des installations éoliennes de production d'électricité en mer dans une zone au large de la normandie. https://www.cre.fr/fileadmin/Documents/Actualites/import/230309_2023-77_Instruction_AO4_Rapport_de_synthese.pdf.
65. Eoliennes en Mer. (2024). Centre manche 1 – projet centre manche. https://www.eoliennesenmer.fr/facades-maritimes-en-france/facade-manche-mer-du-nord/projet-centre-manche/centre-manche-1.
66. RTE. (2023). 2023 electricity report – production — rte (Éolien en mer). https://analysesetdonnees.rte-france.com/bilan-electrique-2023/production#Eolienenmer.
67. Eoliennes en Mer. (2024). Projet en sud-atlantique. https://www.eoliennesenmer.fr/facades-maritimes-en-france/facade-sud-atlantique/projet-en-sud-atlantique.
68. Eoliennes en Mer. (2024). Études sur la zone – projet en sud-atlantique. https://www.eoliennesenmer.fr/facades-maritimes-en-france/facade-sud-atlantique/projet-en-sud-atlantique/etudes-zone.
69. Vollmer, L., and Dörenkämper, M. (2023). Ad-Hoc Analyse: Modellierung des Ertrags eines weiteren langfristigen Ausbauszenarios für den Flächenentwicklungsplan 2023. Tech. Rep. Fraunhofer-Institut für Windenergiesysteme Bremerhaven https://www.bsh.de/DE/THEMEN/Offshore/Meeresfachplanung/Flaechenentwicklungsplan/_Anlagen/Downloads/Annex_Begleitgutachten_FEP2023.pdf?__blob=publicationFile&v=1.BSH
70. Bundesamt für Seeschifffahrt und Hydrographie (BSH) (2020). Flächenentwicklungsplan 2020 für die Deutsche Nord- und Ostsee (Bundesamt für Seeschifffahrt und Hydrographie Hamburg und Rostock). https://www.bsh.de/DE/THEMEN/Offshore/Meeresfachplanung/Flaechenentwicklungsplan/_Anlagen/Downloads/Downloads_Publikationsslider/FEP_2020_Flaechenentwicklungsplan_2020.pdf?__blob=publicationFile&v=6.
71. Vollmer, L., and Dörenkämper, M. (2023). Estimation of Long-term Offshore Wind Energy Yield in the German EEZ (Fraunhofer IWESb). https://www.bsh.de/EN/TOPICS/Offshore/Sectoral_planning/_Anlagen/Downloads/Estimation_of_long_term_offshore_wind_energy_yield_in_the_German_EEZ.pdf?__blob=publicationFile&v=2.BSH.
72. Dörenkämper, M., Meyer, T., Baumgärtner, D., Borowski, J., Deters, C., Dietrich, E., Fricke, J., Hans, F., Jersch, T., Leimeister, M., et al. (2023). Endbericht: Flächenentwicklungsplan 2023 Beratung – Weiterentwicklung der Rahmenbedingungen zur Planung von Windenergieanlagen auf See und Netzanbindungssystemen. Bundesamt für Seeschifffahrt und Hydrographie (BSH). 78, D-20359. https://www.bsh.de/DE/THEMEN/Offshore/Meeresfachplanung/Flaechenentwicklungsplan/_Anlagen/Downloads/FEP_2023_1/Endbericht_FEP_2023_Beratung.pdf.
73. Dörenkämper, M., Meyer, T., Baumgärtner, D., Borowski, J., Deters, C., Dietrich, E., Fricke, J., Hans, F., Jersch, T., Leimeister, M., et al. (2022). Zweiter Zwischenbericht: Flächenentwicklungsplan 2022 Beratung - Weiterentwicklung der Rahmenbedingungen zur Planung von Windenergieanlagen auf See und Netzanbindungssystemen. Bundesamt für Seeschifffahrt und Hydrographie (BSH). 78, D-20359. https://www.bsh.de/DE/THEMEN/Offshore/Meeresfachplanung/Flaechenentwicklungsplan/_Anlagen/Downloads/FEP_2022_2/Zweiter_Zwischenbericht_FEP-Beratung.pdf.
74. Bundesamt für Seeschifffahrt und Hydrographie (BSH). (2024). Stellungnahme des bsh: Aktueller planungsstand des flächenentwicklungsplans im kontext netzentwicklungsplan strom 2037/2045 und ausschreibungen windenergie auf see 2024. https://www.bsh.de/DE/THEMEN/Offshore/Meeresfachplanung/Flaechenentwicklungsplan_2025/Anlagen/Downloads/Stellungnahme_BSH_Planungsstand_FEP.html.
75. Federal; Maritime; Hydrographic Agency (BSH) (2025). Site development plan 2025 for the german north sea and baltic sea. Tech. Rep. (Federal Maritime and Hydrographic Agency [BSH]) https://www.bsh.de/EN/TOPICS/Offshore/Sectoral_planning/sectoral_planning_node.html
76. Bundesamt für Seeschifffahrt und Hydrographie (BSH). (2025). Flächenentwicklungsplan 2025 für die deutsche nordsee und ostsee. Tech. Rep. https://www.bsh.de/DE/THEMEN/Offshore/Meeresfachplanung/Flaechenentwicklungsplan_2025/flaechenentwicklungsplan_2025_node.html pDF.
77. Vollmer, L., and Dörenkämper, M. (2024). Ad-hoc analyse: Ertragsmodellierung der ausbauszenarien 16 bis 21. Tech. Rep. 10-11790 (Fraunhofer-Institut für Windenergiesysteme). https://www.bsh.de/DE/THEMEN/Offshore/Meeresfachplanung/Flaechenentwicklungsplan_2025/Anlagen/Downloads/Adhoc_Analyse_Ertragsmodellg.pdf?__blob=publicationFile&v=2.
78. Vollmer, L., and Dörenkämper, M. (2025). Ad-hoc analyse: Ertragsmodellierung der ausbauszenarien 24 und 25.https://www.bsh.de/DE/THEMEN/Offshore/Meeresfachplanung/Flaechenentwicklungsplan_2025/Anlagen/Downloads_FEP2025/Adhoc_Analyse_Ertragsmodellg_24_25.html.
79. Vollmer, L., Sengers, B.A.M., and Dörenkämper, M. (2024). Brief communication: A simple axial induction modification to the Weather Research and Forecasting Fitch wind farm parameterization. Wind Energy Sci. *9*, 1689–1693. https://doi.org/10.5194/wes-9-1689-2024.
80. Bureau of Ocean Energy Management (BOEM). (2024). Atlantic shores south – renewable energy state activities. https://www.boem.gov/renewable-energy/state-activities/atlantic-shores-south.
81. U.S. Department of the Interior, Bureau of Ocean Energy Management, U.S. Department of Commerce, National Oceanic and Atmospheric Administration, National Marine Fisheries Service, U.S. Department of Defense, and U.S. Army Corps of Engineers (2024). Record of decision: Atlantic shores offshore wind south project - construction and operations plan (U.S. Department of the Interior). https://www.boem.gov/sites/

default/files/documents/renewable-energy/state-activities/Atlantic%20Shores%20South%20ROD.pdf.

82. Atlantic Shores Offshore Wind (2024). Construction and operations plan: Lease area ocs-a 0549 - atlantic shores north, volume i project information. 45600 (Sterling Publishers). https://www.boem.gov/sites/default/files/documents/renewable-energy/state-activities/new-jersey/Atlantic%20Shores%20North_OCS-A%200549_COP%20Volume%20I_03-01-2024.pdf.
83. Bureau of Safety and Environmental Enforcement (BSEE) (2024). Bsee national renewable energy operations map (final) (Bureau of Safety and Environmental Enforcement [BSEE]). https://www.bsee.gov/sites/bsee.gov/files/2024-07/2024_07_17%20-%20BSEE%20National%20Renewable%20Energy%20Operations%20Map%20%28Final%29.pdf.
84. U.S. Department of the Interior (DOI). (2024). Biden-harris administration approves ninth offshore wind project. https://www.doi.gov/pressreleases/biden-harris-administration-approves-ninth-offshore-wind-project.
85. Bureau of Ocean Energy Management (BOEM) (2024). Renewable energy lease and grant information (US Department of the Interior, Bureau of Ocean Energy Management [BOEM]). https://www.boem.gov/renewable-energy/lease-and-grant-information.
86. Bureau of Ocean Energy Management (BOEM). (2024). New Jersey activities - renewable energy state activities. https://www.boem.gov/renewable-energy/state-activities/new-jersey-activities.
87. 3E. (2021). LCOE offshore wind in the Princess Zone: Analysis of various density scenarios. Tech. Rep. https://economie.fgov.be/sites/default/files/Files/Energy/LCOE-offshore-wind-in-the-Princess-zone.pdf.
88. 3E. (2024). Offshore wind at the princess elisabeth zone: Ex-ante analysis of the cfd strike price. Tech. Rep. https://economie.fgov.be/sites/default/files/Files/Energy/Offshore-wind-at-the-Princess-Elisabeth-Zone-Ex-ante-analysis-of-the-CfD-strike-price.pdf.
89. Federal Public Service Economy, SMEs, Self-Employed and Energy. (2024). Belgian offshore wind energy. https://economie.fgov.be/en/belgian-offshore-wind-energy.
90. AFRY Netherlands BV. (2024). Offshore wind energy market study – implications for tenders ijmuiden ver gamma and nederwiek i. Tech. Rep. https://english.rvo.nl/sites/default/files/2024-09/Offshore_Wind_Energy_Market_Study_April_2024_2.pdf.
91. Stehly, T., and Beiter, P. (2019). 2018 cost of wind energy review. Tech. Rep. NREL/TP-5000-74598 (National Renewable Energy Laboratory [NREL])). https://www.nrel.gov/docs/fy20osti/74598.pdf.
92. Stehly, T., Beiter, P., and Duffy, P. (2020). 2019 cost of wind energy review.. Tech. Rep. NREL/TP-5000-78471 (National Renewable Energy Laboratory [NREL]) https://www.nrel.gov/docs/fy21osti/78471.pdf.
93. Stehly, T., and Duffy, P. (2022). 2020 cost of wind energy review. Tech. Rep. NREL/TP-5000-81209 (National Renewable Energy Laboratory [NREL]). https://www.nrel.gov/docs/fy22osti/81209.pdf.
94. Stehly, T., and Duffy, P. (2022). 2021 cost of wind energy review. Tech. Rep. NREL/TP-5000-84774 (National Renewable Energy Laboratory [NREL]). https://www.nrel.gov/docs/fy23osti/84774.pdf.
95. Stehly, T., Duffy, P., and Hernando, D.M. (2023). 2022 cost of wind energy review.. Tech. Rep. NREL/TP-5000-88335 (National Renewable Energy Laboratory [NREL]) https://www.nrel.gov/docs/fy24osti/88335.pdf.
96. Stehly, T., Duffy, P., and Hernando, D.M. (2024). Cost of wind energy review: 2024 edition. Tech. Rep. NREL/TP-5000-91775 (National Renewable Energy Laboratory [NREL]). https://www.nrel.gov/docs/fy25osti/91775.pdf.
97. Kost, C., Shammugam, S., Jülch, V., Nguyen, H.T., and Schlegl, T. (2018). Levelized cost of electricity – renewable energy technologies.. Tech. Rep. (Fraunhofer Institute for Solar Energy Systems ISE) https://www.ise.fraunhofer.de/content/dam/ise/en/documents/publications/studies/EN2018_Fraunhofer-ISE_LCOE_Renewable_Energy_Technologies.pdf
98. Kost, C., Shammugam, S., Fluri, V., Peper, D., Memar, A.D., and Schlegl, T. (2021). Levelized cost of electricity – renewable energy technologies. Tech. Rep. (Fraunhofer Institute for Solar Energy Systems ISE) https://www.ise.fraunhofer.de/content/dam/ise/en/documents/publications/studies/EN2021_Fraunhofer-ISE_LCOE_Renewable_Energy_Technologies.pdf
99. Kost, C., Müller, P., Schweiger, J.S., Fluri, V., and Thomsen, J. (2024). Levelized cost of electricity – renewable energy technologies. Tech. Rep. (Fraunhofer Institute for Solar Energy Systems ISE) https://www.ise.fraunhofer.de/content/dam/ise/en/documents/publications/studies/EN2024_ISE_Study_Levelized_Cost_of_Electricity_Renewable_Energy_Technologies.pdf
100. BVG Associates, and Offshore Renewable Energy (ORE) Catapult. (2024). Guide to an offshore wind farm. Tech. Rep. https://guidetoanoffshorewindfarm.com/.
101. Badouard, T., de Oliveira, D.M., Yearwood, J., and Torres, P. (2020). Final report – lcoe & lcoh: Energy costs, taxes, and the impact of government interventions on investments. Tech. Rep. TEC1204EU. https://energy.ec.europa.eu/system/files/2020-10/final_report_levelised_costs_0.pdf.
102. International; Renewable; Energy Agency (IRENA) (2024). Renewable power generation costs in 2023.. Tech. Rep. (International Renewable Energy Agency [IRENA]) https://www.irena.org/-/media/Files/IRENA/Agency/Publication/2024/Sep/IRENA_Renewable_power_generation_costs_in_2023.pdf
103. Johnston, B., Foley, A., Doran, J., and Littler, T. (2020). Levelised cost of energy, A challenge for offshore wind. Renew. Energy *160*, 876–885. https://www.sciencedirect.com/science/article/pii/S0960148120309241.
104. Department; Energy; Security; Net; Zero (DESNZ) (2023). Electricity generation costs 2023. Tech. Rep. (UK Government - Department for Energy Security and Net Zero [DESNZ]) https://assets.publishing.service.gov.uk/media/6556027d046ed400148b99fe/electricity-generation-costs-2023.pdf